Nanoplastic cleanup during drinking water treatment: uncovering the potential of coagulation-flocculation-sedimentation

Understanding the influence of particle size, coagulant type and coagulant dose on nanoplastic removal during coagulation-flocculation-sedimentation

TUDelft

MSc Thesis
Ine Vroman

Nanoplastic cleanup during drinking water treatment: uncovering the potential of coagulation-flocculation-sedimentation

Understanding the influence of particle size, coagulant type and coagulant dose on nanoplastic removal during coagulation-flocculation-sedimentation

By

Ine Hilde Vroman
Student ID: 5381444

in partial fulfilment of the requirements for the degree of
Master of Science
in Environmental Engineering
at the Faculty of Civil Engineering of Delft University of Technology

September 2024

Supervisors:	Dr. Ir. Kim Maren Lompe
	Februriyana Pirade
Thesis committee:	Dr. Ir. Kim Maren Lompe, TU Delft (Chair)
	Prof. Dr. Ir. Merle de Kreuk, TU Delft (External)
	Februriyana Pirade, TU Delft (Daily Supervisor)

Cover: earth.com

TUDelft

Acknowledgements

Abstract

Microplastic (MP, < 5 mm) and nanoplastic (NP, < 1 μm) pollution has become a growing environmental concern, as they are detected everywhere, including in surface waters used for drinking water (DW) production. Recently, NPs have been detected in finished DW, indicating incomplete removal by DW treatment plants (DWTPs). Coagulation-flocculation-sedimentation (CFS) is a promising treatment technique, but current research lacks connection to practice and/or mostly focuses on MPs. This thesis investigates the influence of coagulant type, dose, and NP size on NP removal during CFS. The research connects to practice by using coagulants and doses used in the Dutch DWTPs.

A survey with four Dutch DW companies provided insight into the CFS procedures. Jar tests simulated CFS in the lab, using ferric chloride ($FeCl_3$), aluminium chloride ($AlCl_3$) and polyaluminium chloride (PAC) to assess the impact of coagulant types. Theoretical optimum doses were compared to practical doses (obtained from survey) to determine the influence of the coagulant dose. Lastly, the effect of NP sizes on CFS removal efficiencies was studied using 200, 500, and 1000 nm NPs. All experiments were done with NPs spiked in tap water. CFS efficiency was evaluated through turbidity, pH, alkalinity, UV-VIS, residual coagulant and ζ-potential measurements.

PAC was identified as the most efficient coagulant considering all evaluated parameters. Theoretical doses, which were higher than practical doses for $FeCl_3$ and $AlCl_3$, achieved more effective NP removal than practical doses. Charge neutralisation was confirmed as the main mechanism for NP removal. Lastly, although particle size is generally thought to affect NP removal, this study's results did not allow for confirmation or refutation of this statement. Overall, this research highlights that the type of coagulant and dose can influence NP removal in DWTPs. These findings can be a first step to help DWTPs optimise CFS for more NP removal.

Keywords: *nanoplastic, nanoplastic size, coagulation-flocculation-sedimentation, coagulant type, coagulant dose, ferric chloride ($FeCl_3$), aluminium chloride ($AlCl_3$), polyaluminium chloride (PAC), drinking water companies*

Contents

List of Figures

List of Tables

List of Equations

List of Abbreviations and Symbols

Abbreviation	Definition
CF	Coagulation-flocculation
CFS	Coagulation-flocculation-sedimentation
DW	Drinking water
DWC	Drinking water company
DWD	Drinking Water Directive
DWT	Drinking water treatment
DWTP	Drinking water treatment plant
GW	Groundwater
ICP-OES	Inductively coupled plasma optical emission spectrometry
JT	Jar test
LOD	Limit of detection
MP	Microplastic
MW	Molecular weight
NOM	Natural organic matter
NP	Nanoplastic
NTU	Nephelometric turbidity units
PA	Polyamide
PAC	Polyaluminium chloride
PAM	Polyacrylamide
Pd	Palladium
PE	Polyethylene
PET	Polyethylene terephthalate
Poly-DADMAC	Polydiallyldimethyl ammonium
PP	Polypropylene
PS	Polystyrene
PVC	Polyvinylchloride
RBF	Riverbank filtrate
RQ	Research question
SA	Surface area
SF	Sand filtration
SW	Surface water
UV-VIS	Ultraviolet–visible light
WHO	World health organization
WWTP	Wastewater treatment plant
HA	Humic acid

Symbol	Definition	Unit
ζ	Zeta-potential	mV
C	Mass concentration	mg/L
V	Volume	L or m³
N	Normality	eq/mol
M	Molarity	mol/L
ρ	Density	g/L or g/cm³
r	Radius	m
A	Area	m²
m	Mass	G
R%	Removal efficiency	%

Chapter 1
Introduction

At this point in modern life, we touch plastic more than we touch our loved ones. Plastic is everywhere: it is in our air, our water, and in our soils. [...] We are just beginning to understand the effects of our global reliance on this material. What makes plastic useful is exactly what makes it harmful: it persists.

~ The Plastic Atlas

Plastic is omnipresent in modern society due to its favourable properties: cheap, strong, lightweight, durable, resistant to degradation and good insulation to heat and electricity [2]. Approximately 400 million tonnes are produced per year [3]. 9.2 billion tonnes of plastic were produced between 1950 and 2017, which is more than one tonne for each person currently living on this planet. Most plastics are intended for single-use [4], making plastic the greatest pollutant worldwide [5].

Each year 9 to 23 million metric tonnes of plastic waste enter oceans, lakes and rivers [3]. Plastics in aquatic environments undergo chemical modifications, mechanical abrasion and photodegradation. As a result, plastic breaks up into smaller particles; microplastics (MPs, < 5 mm) and nanoplastics (NPs, < 1 μm) [2, 3, 6]. These particles are stable and accumulate in the ecosystem, including rivers, lakes and groundwater used for the production of drinking water (DW) [5]. Concerns about potential adverse health effects from MP/NP ingestion through the food chain and drinking water [7, 8] have prompted environmental engineers to focus on fighting the pollution brought by this (emerging) contaminant [9].

Studies show that MPs and NPs are present in DW. However, concentrations are lower in tap water than in untreated source water, indicating removal by drinking water treatment plants (DWTPs) [5, 8, 10]. The mechanisms have not been systematically studied so far [3, 8]. Physicochemical processes like adsorption, (membrane) filtration and coagulation-flocculation-sedimentation (CFS) are currently used in water treatment to remove dissolved and particulate contaminants [3, 11]. Especially coagulation-flocculation (CF) has received much attention for removing MPs and NPs from polluted streams, because of the simplicity, low carbon footprint and low operational costs [2].

Surface water (SW) treatment plants typically consist of at least a conventional treatment line. The core of conventional treatment is particle removal via CFS. The selection of coagulant type and dose is influenced by water quality parameters such as particle composition and turbidity. The process efficiency can be increased with coagulant aids and/or flocculant aids. The primary goal of conventional coagulation is to remove turbidity (inorganic colloidal particles), but coagulation can be enhanced to remove both turbidity and natural organic matter (NOM) [12, 13].

Given that the CFS process is defined by the used chemicals and the targeted particles, this master's thesis aims to determine and understand the effect of NP size, coagulant type and coagulant dose on the removal efficiency (R%) of NPs via CFS. Three research questions (RQ) guide this research:

RQ1: How do different coagulant types compare in removing nanoplastics?
RQ2: How does the variation in coagulant dose affect the nanoplastic removal efficiency?
RQ3: To what extent does variation in NP particle size affect the nanoplastic removal efficiency?

Chapter 2 provides the theoretical background, covering plastics in the aquatic environment, current DW production practices, potential (nano)plastic removal technologies and the CF mechanisms involved in plastic removal. Chapter 3 describes the material and methods used and followed during this thesis. The results are presented in Chapter 4 and the discussion follows in Chapter 5. Chapter 6 summarises this research, while Chapter 7 concludes the thesis by zooming in on possibilities and recommendations for future research.

Chapter 2
Theoretical background

2.1. Plastics in the (aquatic) environment

The plastic revolution started with the invention of parkensine (1850s), bakelite (1907), polyvinyl chloride (PVC, 1920s) and nylon (polyamide, PA, 1940s) [14] but today there is a wide variety of plastic products for different applications. The monomers can be fossil- or biomass-based depending on the origin of the carbon source [15, 16] and the final product can be altered by additives like flame retardants, plasticisers, fillers, lubricants, pigments, and heat stabilisers [16-18]. PVC, polyethylene (PE) and polypropylene (PP) are currently the most popular plastic types, but polyethylene terephthalate (PET) and polystyrene (PS) are also commonly used [4, 19]. With a significant portion of the plastics intended for single use, it is estimated that over 60 % of all plastics ever produced have been discarded into landfills or the environment [19, 20]. As a result, plastic pollution is now a crucial environmental problem [8, 21].

Plastic can enter the aquatic environment as larger debris, or already as smaller MP/NPs. The larger plastic debris (bags, packaging material, ropes, …) is easily moved by wind or water due to its lightweight nature [2, 5] and ages and degrades over time. The degradation happens through solar radiation, temperature changes, biodegradation, and mechanical forces. The process depends on physical and chemical properties like polymer shape, size, porosity, surface area (SA), morphology, and water quality. The ability to interact with other contaminants also influences the process [18, 22]. Degradation causes the macroplastics (> 20 mm) to gradually transform into plastics with an increasingly smaller particle size and a rougher surface. Continued degradation leads to MPs (< 5 mm) and eventually to NPs (< 1 µm) [2, 3, 6, 23]. Increased particle SA facilitates the release of additives and the adsorption of (toxic) organic pollutants (aromatic hydrocarbons, polychlorinated biphenyls, phthalates) and heavy metals (Zn, Pb, Cu) [2, 18, 24]. Consequently, the longer plastic remains in the water, the more diverse the array of particles and released chemicals. Compared to larger debris the smaller particles are more mobile and accessible for uptake in organisms [24].

Another pollution type are the primary and secondary MPs/NPs that enter the aquatic environment mostly via stormwater runoff, treated wastewater treatment plant (WWTP) discharge, or WWTP biosolids used as fertiliser. Primary MPs are intentionally produced as components for commercial products. The most well-known examples are microbeads produced for cosmetics [5, 18]. Secondary MPs result from the breakdown of larger aged plastics. Common sources include tyre wear and clothing fibres released during washing [5, 16]. MPs that enter WWTPs can fragment further into NPs due to extensive mixing, pumping and the addition of oxidants [25].

The MP/NP research field is relatively new and the implications of its presence in water are a hot topic in current research. The first observation of 'small plastic particles' in open ocean dates back to the 1970s, but the term MP was not coined until 2004 [16]. NPs were first detected in an aquatic environment in 2017 by Ter Halle et al. (2017) in the North Atlantic subtropical gyre [26]. By now, MPs and NPs have been detected in both urban and remote locations [19]. As MPs and NPs pollute the aquatic environment, these particles also contaminate the food chain and DW (sources) [5, 8]. For this reason, the widespread occurrence of MPs and NPs has raised scientific and public concern [2].

Earlier studies often considered NPs as an extension of MPs due to their similar origin and composition. However, new research reveals significant differences in analytical complexities, transport characteristics, pollutant interactions, biological effects, removal behaviours, and health concerns [7, 25]. Conclusions based on MP research should be considered for NP research but cannot be directly translated into conclusions for NPs.

2.1.1. Microplastics versus nanoplastics in the aquatic environment

Transport patterns and fate in (urban) water systems differ significantly between MPs and NPs. For example; the settling rate of a PVC bead (1.4 g/cm³) with size 2 mm and 100 nm respectively equals 87 cm/s and 6.9 cm/year under ideal conditions (Stokes' law) [7]. Plastic aggregation also varies. Plastic particles can aggregate with themselves (homo-aggregation) or with colloids like clay, algae, dissolved organic matter and anthropogenic materials (hetero-aggregation). Aggregation is controlled by particle size, surface properties, surrounding colloids and ionic strength of the water. The Derjaguin-Landau-Verwey-Overbeek theory (stability of colloidal dispersions) suggests that larger particles are less likely to aggregate, resulting in higher stability and mobility. Environmental conditions like high salinity or the presence of extracellular polymeric substances respectively influence the aggregation positively and negatively. These factors have a bigger influence on NPs than on MPs due to the more outspoken surface properties [7].

NPs interact more strongly with other pollutants than MPs, owing to the higher surface-to-volume ratio and the abundant surface functional groups. Interactions with pollutants like inorganic metal ions and clays, organics, and microbes lead to the formation of composite pollutants. These composite pollutants can influence the transport mechanisms, the toxicity, analysis and removal of plastics. The main drivers of these interactions include van-der-Waals forces, hydrophobic/hydrophilic interaction, pore-filling interaction, hydrogen bonding, surface complexation, electrostatic interaction, and π-π. Consequently, the size, available SA and functional groups of the plastics play a big role in these interactions [7].

The interaction between MPs/NPs and metal ions and NOM also varies. MPs adsorb metal ions on the surface depending on sorption capacity (MPs porosity, SA and morphology), while interaction between NPs and metal ions results in the compression of the electrical double layer of the NP. This in turn leads to the aggregation of NPs. Aggregation is more likely when exposed to high valence metal ions like Fe^{3+} than when exposed to low valence metal ions like Na^+. NOM is abundantly present in natural waters, and has different chemical groups (e.g., -OH, -COOH, and phenolic groups). NOM interactions with MPs/NPs involve additional complex interactions such as hydrophobic interactions and bridging, affecting surface properties. Some studies suggest that these interactions could improve the aggregation of MPs, while other studies suggest that the interactions had a negligible effect on MP aggregation. The effect of NOM on the aggregation of dispersed NPs is generally considered to be little. However, the effect is influenced by coexisting substances in the waters [7, 22].

2.1.2. Concerns about the ecological and human impact

The environmental and health impacts of MPs/NPs are still being studied, but the consequences are potentially far-reaching [27]. The fact that the plastic particles interact with other (toxic) contaminants and heavy metals increases those concerns, because of the bioaccumulation of toxins. Adsorbed pollutants can affect metabolic and physiological processes and pose threats to human and ecological health [2, 6, 27]. For these reasons, MPs were listed by the United Nations Environment Programme (UNEP) as one of the top ten emerging important pollutants [10].

Over 690 aquatic species have been affected by MPs [8]. Research shows that exposure to MPs can cause oxidative damage, growth inhibition, liver toxicity, immune stress, and reduced feeding activity [8, 10]. Smaller particles are more mobile and accessible for uptake in organisms compared to larger debris [24]; e.g. blue mussel larvae internalise 100 nm NPs six to ten times more than 2 µm MPs [2, 10, 28]. The symptoms related to NP exposure were similar to the effects of MP exposure, but embryotoxicity reduced fertility and damage to the digestive system were observed as extra symptoms [8, 29]. NPs have also been detected in fish brain tissue, indicating that the NPs can cross the blood-brain barrier. NP accumulation in the fish brain can result in behavioural disorders and oxidative DNA damage [8, 28].

MPs can enter the human body through ingestion and inhalation. Individuals ingest approximately 5800 particles of synthetic debris each year. The majority (88 %) originates from DW [20, 21], but other sources are aquatic organisms and table salt. This leads to gastrointestinal exposure [2, 8]. MPs can also enter the respiratory system, through inhalation of MPs suspended in the air. Knowledge of the adverse effects of MPs on the human body is limited [8], but laboratory tests with mice and dogs suggest that health impacts could include endocrine disruption, irritation to the alveoli (< 135 nm) and particle deposition in lymph nodes (< 130 nm), liver, kidney, and gut (< 20 mm). Particles smaller than 110 nm were found in the blood, urine, and cerebrospinal fluid in dog studies. The accumulation and deposition were inversely proportional to the MP particle size [27]. In vitro studies with PS NPs indicate induced activation of cell responses and immune responses [8]. Research suggests that alternations found in animal models can be extrapolated to humans. This would mean the gut microbiota is affected by NPs, negatively affecting the immunological, endocrine and neurological system [29]. Long-term studies on repeated exposures to different plastic materials are missing in literature [8], but considering current findings, the particles should be removed from our DW and food chain as much as possible.

2.2.   (Nano)plastics in drinking water and drinking water treatment plants

2.2.1.   (Nano)plastics and drinking water quality

There is an ongoing debate within the scientific community regarding the health implications of plastic exposure through DW. While the World Health Organization (WHO) has indicated a low health concern related to MP exposure via DW (2019), studies show significant concern regarding smaller particles. The effects most likely depend on host susceptibility, exposure time and intensity. Therefore, it is the concentration of plastic particles per volume of beverage that is important to assess the risks [5]. Surveys show MPs present in 81 % of tap water samples (129/159) across multiple countries and 93 % of bottled water samples (241/259) from 11 brands [21]. The abundance in bottled water is 10 times higher than in tap water [30].

DW (tap water in this context) must meet several criteria to be considered safe for consumption. The legal requirements in the Netherlands can be found in the Drinking Water Decree (Drinkwaterbesluit) and are based on the European Drinking Water Directive (DWD). The European DWD was first enacted in 1998 but has been reviewed in 2016 considering technical and scientific progress. Changes in the DWD were adopted in 2020 and the updated decree took effect from January 2021 on European level and from January 2023 on Dutch level. The revised DWD includes a watch list to address the growing public concerns about emerging pollutants, including MPs [31]. The watch list allows dynamic and flexible responses to follow-up new knowledge regarding the best-practice monitoring approaches and methodologies, as well as new developments regarding the pollutant's relevance to human health [32].

The DWD implies that Member States should pay special attention to MPs and endocrine-disrupting compounds where SWs are used to produce DW. Where necessary, the Member States can require water suppliers to monitor and treat MPs and other parameters included in the watch list [32]. In the Netherlands, measurement obligations have been implemented for MPs [31], but there are currently no established legal limits [8]. Studies and laws for plastics in DW are mainly related to particles bigger than 1 mm, because NPs were only described recently (2017) and because the smaller particles are posing more challenges with analytical detection limits [5], e.g. environmental samples need to be concentrated up to 10^8 times to meet the minimal NP detection limit of flow cytometry [30].

2.2.2.   (Nano)plastic removal in drinking water treatment plants

A limited number of studies have focussed on plastics in DWTPs. There is limited data available on how MPs and NPs behave during treatment, leaving many questions unanswered [21]. Studying NP removal is challenging due to difficulties in NP identification, analysis, and quantification [25, 29]. These challenges arise from their small size, density similar to water, time-consuming extraction methods for quantification, and NOM-modified surface. These factors make it difficult to quantify MPs and NPs in real-time at full-scale DWTPs [33]. Some studies have been able to report MP/NP concentrations in SWs between 0.006 and 699 μg/L depending on the location [8, 10, 15, 30]. PS, PVC and PA-based NPs with a size between 58-255 nm are most abundantly found in tap water (1.67 to 2.08 μg/L) [10]. The concentrations before and after treatment indicate that removal is not perfect but that it takes place at DWTPs. This section therefore briefly reviews the (non-)conventional techniques possibly involved in MP/NP removal.

Kumar et al. (2023) reviewed different studies and compared the overall MP removal efficiency (R%) in DWTPs. 70 % MP removal was observed in a DWTP operating with CF followed by sand filtration (SF). 81 % was removed in a different DWTP using CFS followed by SF. A third DWTP achieved a removal rate of 83 % with flotation, SF, and activated carbon filtration [8]. Arenas et al. (2021) performed the first full-scale study on NP removal in conventional DWTPs and reported an NP R% of 99.4 % for positively charged PS amidine NPs. The removal rates of the individual steps are unknown for these DWTPs [34]. Additional (laboratory) research, mimicking the operating conditions at DWTPs, is required to help understand the fate of plastic particles in these processes individually [8].

In the Netherlands, DW is produced from groundwater (GW, 55 %), (dune infiltrated) SW (40 %) and riverbank filtrate (RBF, 5 %). The production of DW is a multi-step process, visualised in Figure 1. SW contains the highest MP/NP concentration [15] and the treatment processes include (1) intake of SW, possible pre-treatment by storage in natural reservoirs, (2) particle removal by micro-screens and CF, (3) floc removal with double-layer filters, (4) main disinfection with ultraviolet (UV) light, (5) removal of odour and colour with activated carbon filters and lastly (6) storage of the water after possible pH adjustment and oxidation [35]. Currently, there are no steps in the treatment specifically focussing on MP/NP removal [8]. However, since MPs/NPs are particles, existing processes designed to remove dissolved and particulate contaminants, such as filtration, CFS and adsorption are receiving the most attention [8, 11, 20, 23].
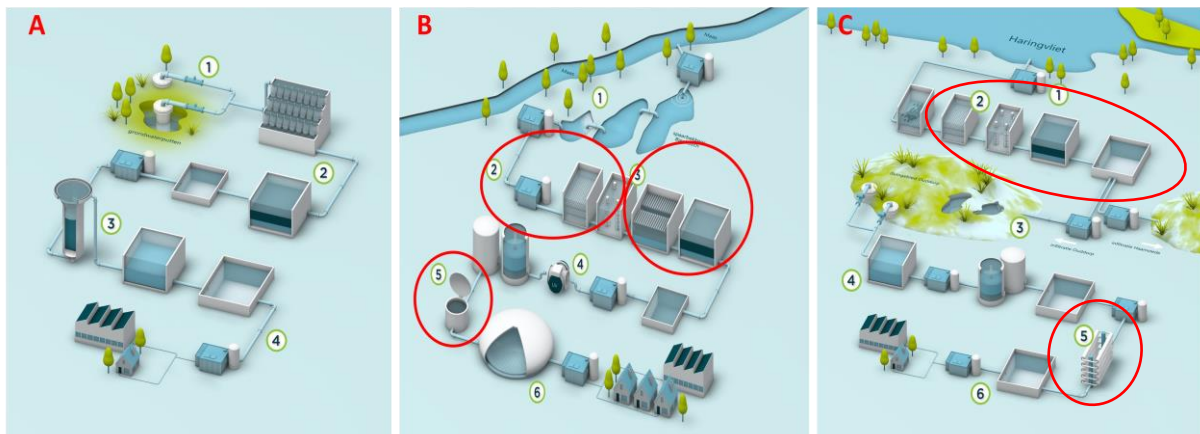
Figure 1: Treatment trains for production of drinking water from groundwater (A), surface water (B) and infiltrated (dune) water (C). The technologies considered for MP/NP removal are encircled.

2.2.2.1. Filtration techniques

Filtration technologies can be categorised as media filtration techniques or membrane filtration techniques. The most common media filtration technique is (rapid) SF. This is part of the conventional treatment train used in DWTPs and aims to remove particles, iron and manganese [35, 36]. MP research indicates that SF can remove MPs larger than 10 µm with an efficiency of 29.0-44.4 %, but smaller particles often remain in the effluent [37]. NP research found a R% of 19 % and 16 % for PS NPs of 20 nm and 200 nm respectively. Biofilm formation in the quartz sand increased the R% to 42 % and 82 %, respectively. Additionally, a full-scale experiment with positively charged PS amidine NPs showed a R% of 54.3 ± 3.1 % [34].

Membrane filtration includes microfiltration (100-1000 nm), ultrafiltration (10-100 nm), nanofiltration (1-10 nm) and reverse osmosis (0.1-1 nm) [36, 37]. Micro- and nanofiltration are used to remove colloids by physical sieving, but this is not (yet) part of the common treatment line [36, 38]. The process (efficiency) depends on the membrane pore size, the membrane properties and the particle properties [29]. Gao et al. (2022) report that ultrafiltration can completely remove all PE MPs without any co-treatment process because the MPs are bigger than the membrane pore size. The same result was found for PS microbeads [37]. Nano- and ultrafiltration membranes effectively adsorb and remove NPs, because the negatively charged NPs adsorb to the positively charged groups of the membranes. Keerthana Devi et al. (2022) reviewed multiple studies to find that membranes with an increasingly smaller pore size achieve higher NP R% (3, 0.70 and 0.22 µm filter pore correspond to an NP R% of 32 ± 12 %, 84 ± 3 % and 92 ± 3 % respectively) [29].

Size exclusion is the main principle of membrane filtration, but other factors like pore blocking and fouling also influence the retention. These phenomena allow particles larger than the pore size to move through the membrane, or particles smaller than the pore size to be rejected [29, 36]. Fouling occurs during mass transport because particles accumulate or adsorb in the membrane pores or on the membrane surface. Cleaning steps (e.g. backwash/air flush, chemical cleaning) are required to avoid fouling and to ensure the membrane operates accordingly. This leads to higher operating costs, either by the addition of chemicals or the replacement of membranes [39, 40]. High concentrations of small MPs might magnify fouling, while bigger MPs might form a porous filter cake that allows water to pass through at a lower resistance [37].

2.2.2.2. Adsorption techniques

Adsorption is used to remove contaminants (adsorbates) from the water by transferring them to the surface of a solid phase (adsorbent) [41]. The transfer is facilitated by electrostatic interactions, hydrogen bonds and π-π interactions [37]. Typically, adsorption targets organic substances, residual inorganic compounds (e.g., heavy metals, nitrogen, sulfides), and micropollutants [42]. Adsorption techniques are generally cheap, highly efficient and easy to operate and implement. Various solids can serve as adsorption material. The materials can be recovered and reused after regeneration [41].

Gao et al. (2022) reviewed different studies that investigated the removal of plastic particles with adsorption. The general conclusion was that the adsorption technique is effective in removing small MPs (< 10 µm) and NPs [37], but it is important to note that the reviewed studies used adsorbents that are not (yet) common in DWTPs [41, 42]. The maximum adsorption capacity of synthesised Zn-Al layered double hydroxides was 164.49 mg/g for 55 nm PS MPs, leading to a R% of 96 %. Zirconium metal-organic framework-based foam materials remove poly-methyl methacrylate, PS, and polyvinylidene fluoride MPs with a R% of 85-90 %. Bio-based materials like a sponge made of chitin, aerogel, biochar, and magnetic biochar showed varying R% [37].

The most common adsorbent in DWTPs is activated carbon [42]. Gao et al. (2022) reported an MP R% of 56.8-60.9 %, and a high R% (73.7-98.5 %) for smaller MPs (1-5 µm) [37]. Pivokonsky et al. (2018) reported an MP R% of around 80 %, and Arenas et al. (2021) demonstrated an NP R% of 78-90 % with granular activated carbon adsorption for positively charged PS amidine NPs [34]. Zhang et al. (2020) observed that the efficiency decreased with decreasing particle size [21].

2.2.2.3. Coagulation-flocculation

CF is widely used to remove inorganic colloidal particles (conventional operation) and NOM (enhanced coagulation) [43]. The treatment step consists of interlinked chemical and physical processes [44] that alter the surface charge of naturally stable particles in suspensions. This alternation leads to destabilisation and facilitates particle aggregation into flocs. These flocs can be removed through floatation, filtration or sedimentation [12].

The CFS process varies across DWTPs because the choice of coagulant type and dose depends on the water quality and composition. Coagulant aids or flocculant aids can be added to enhance the process [12], pH can be adjusted [12, 43] and mixing time and intensity can be tailored to create the desired flocs for subsequent separation [13, 43]. Studies investigating the removal of MPs of various sizes and different polymers (e.g., PE, PS, PEST, PVA, PES, PVC, PET) have reported R% ranging from 1.7 % to 100 %, depending on the coagulants used, the dosages, and the enhancement with coagulant and/or flocculant aids. NP research is more limited. Current findings are mostly based on research with PS NPs between 100 nm and 1 µm. The obtained R% higher than 80 % are promising, but the specific coagulant types, coagulant doses and/or used sedimentation times do not fully align with industry practices [2].

CFS is the most basic and widespread process among the treatment steps considered for MP/NP removal. It is simple and cheap in operation and part of every conventional treatment line [2, 11]. Even though the process is designed to remove particles, the numbers show that MPs/NPs are not completely removed yet. Since the operational efficiency is influenced by several parameters (chemical use, treatment time, stirring speed, pH, temperature, water quality (particularly turbidity and organic content)), many research gaps remain [2, 20, 37]. More specifically this thesis focuses on the influence of coagulant type, coagulant dose and particle size on the achieved NP R%. The next section will therefore delve deeper into the current knowledge regarding used chemicals and dominant mechanisms at play in the CFS process.

2.3.   Coagulation-flocculation and (nano)plastic removal performance

2.3.1.   Coagulants, coagulant aids and flocculant aids in (nano)plastic research

The most common coagulants in current DWTPs are inorganic aluminium or ferric (pre-hydrolysed) salts. Well-known aluminium-based coagulants are aluminium sulfate (alum, $Al_2(SO_4)_3$) and aluminium chloride ($AlCl_3$). Well known iron-based coagulants are ferric sulfate ($Fe_2(SO_4)_3$) and ferric chloride ($FeCl_3$) [12, 43, 45]. Upon addition to water, a chain of reaction occurs between the coagulant, the water and the particulates. These interactions are complex and challenging to control, leading to the development of pre-hydrolysed metal salt coagulants [12, 13]. The most well-known pre-hydrolysed aluminium salt is poly-aluminium chloride (PAC, $Al_a(OH)_b(Cl)_c(SO_4)_d$) [12, 43].

Esfandiari and Mowla (2021) compared Al- and Fe-based coagulants to remove PE MPs from greywater by coagulation and dissolved air flotation. Experiments showed a PE R% of 96.10 % with $AlCl_3.6H_2O$ (14.64 mg/L) and 70.56 % with $FeCl_3.6H_2O$ (13.06 mg/L). This study indicates a difference in MP R% between Al- and Fe-based coagulants [46]. Current research suggests that that difference is smaller for NP removal: 96.6 % and 95.8 % of 50 nm PS-COOH (50 mg/L) were removed by 10 mg/L $AlCl_3$ and $FeCl_3$ respectively [2]. Zhou et al. (2021) showed that 90 mg PAC/L outperforms 90 mg $FeCl_3$/L in the removal of MPs (< 500 µm, 500 mg/L). PS MPs were removed for 77.83 % and 63 % by PAC and $FeCl_3$ respectively [47].

Coagulant and flocculant aids can be used to enhance the coagulation process. Coagulant aids like clay and fine quartz sand are commonly added to waters with low particle concentrations to provide extra nucleating sites. Flocculant aids like (hydrolysed) polyacrylamides and polydiallyldimethyl ammonium (poly-DADMAC), polyacrylamide (PAM), sodium alginate from brown seaweed, etc. increase settleability and filterability of the flocs [12, 43]. Zhang et al. (2021) compared MP R% of 100-400 µm PET (100 mg/L) obtained with 20 mg PAC/L and an increasing dosage of PAM. The R% equalled 35.5 %, 44.47 % and 79.35 % for 0, 5 and 100 mg/L PAM, indicating that coagulant aids increase R% [2, 3, 48].

2.3.2.   Mechanisms involved in (nano)plastic removal

Coagulants neutralise the charges of the suspended particles through (a combination of) multiple mechanisms, including charge neutralisation, polymer bridging, sweep flocculation, and double-layer compression [2]. The first three mechanisms are used in water treatment and are visualised in Figure 2 [2, 3, 6, 12, 38, 45]. Table 1 shows that charge neutralisation is the most common mechanism. The positively charged coagulant hydrolysates interact with the negative charge of particles and MP/NP in solution [13, 43, 45]. These interactions reduce or eliminate the electric repulsion between particles, allowing them to aggregate into flocs [2, 13]. In case the coagulant dosage is higher than the dose required for neutralisation, the particle's charge can be reversed from negative to positive, disturbing the particle removal [12, 13, 45]. Therefore, the point of zero zeta (ζ)-potential is an important indicator of the right coagulant dose [44].

The second main coagulation mechanism is adsorption and interparticle binding, or polymer bridging. This mechanism occurs when using nonionic polymers and high MW, low-surface charge polymers [12]. Different parts of the coagulant's polymeric chain can adsorb to particle surfaces, forming a bridge between the particles. This creates clusters of flocs connected by these polymer bridges [13, 44, 45]. Similar to charge neutralisation, overdosing the coagulant can disrupt the process because it becomes difficult for the polymer to find available vacant adsorption sites on the particle surface [13, 45]. The adsorption processes for plastic particles are currently expected to be driven by hydrogen bonds (MP), hydrophobic interactions, and van der Waals forces (Table 1) [2, 12].

The third coagulation mechanism is sweep flocculation, also known as enmeshment in precipitation. In contrast to the other mechanisms, a coagulant dose higher than required for charge neutralisation is favourable. This higher dose leads to the formation of insoluble precipitates (coagulant flocs) [12, 13, 45]. Particles in the water can become enmeshed or trapped within these precipitates [13, 44, 45]. Sweep flocculation is often mentioned as a mechanism in MP/NP studies when the coagulant dose is higher (Table 1). Ali et al. (2023)' review shows that removal of PE MPs (15 µm and 1-5 µm) with alum doses of 2.73 and 5-10 mg Al/L is respectively facilitated by charge neutralisation and polymer bridging (with PAM) versus sweep flocculation and charge neutralisation. The total CFS time is longer where sweep flocculation occurs (30 minutes) than in the other scenario (8 minutes) [2], underscoring that coagulant flocs have a slower formation rate compared to flocs formed by other mechanisms [44].

Next to the coagulation mechanisms, there are also two general flocculation mechanisms: micro-flocculation (perikinetic flocculation) and macro-flocculation (orthokinetic flocculation) [12]. Micro-flocculation is the main mechanism for particles smaller than 0.1 µm. The flocculation rate of these particles is proportional to the rate at which particles diffuse toward one another. Continuous aggregation of small particles eventually results in the production of microflocs ranging from 1 to 100 µm. Macro-flocculation is the main mechanism for particles bigger than 1 µm. Gentle mixing is important to introduce velocity gradients that cause particle collisions [12, 43]. Considering the size of MPs/NPs, macro-flocculation should dominate in MP removal, while micro-flocculation would play a bigger role in NP removal. However, Abi Farraj et al. (2023) describe macro-flocculation as the major mechanism involved in NP removal [25].
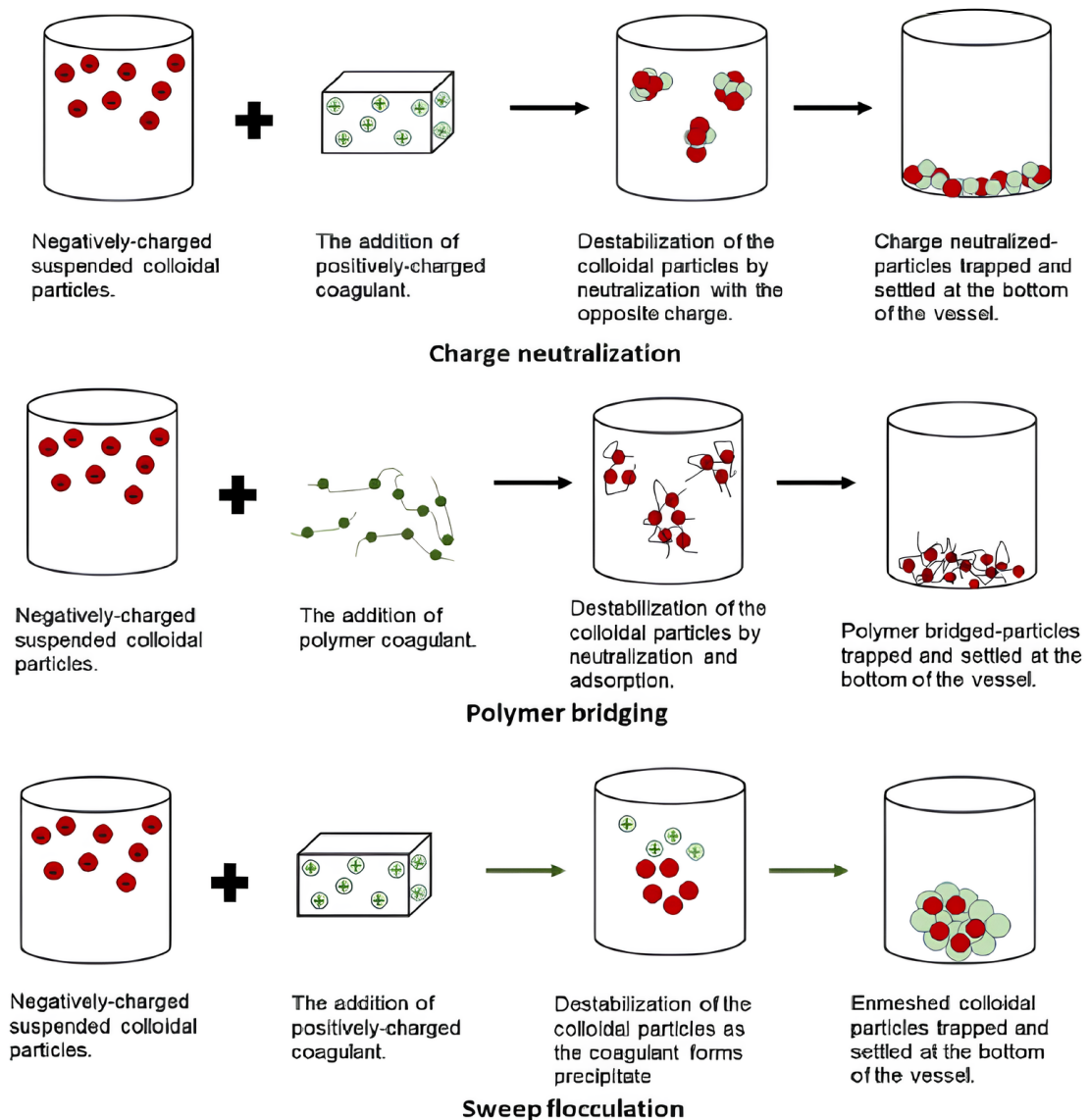
Figure 2: Schematic overview of the coagulation mechanisms involved in MP/NP removal.

2.3.3. Factors influencing coagulation & flocculation efficiency of (nano)plastics

The efficiency of the CF process depends on the selection of coagulant type and the optimal dose but also on the water quality and the operational parameters. The characteristics and concentrations of target impurities, temperature, pH, natural presence of NOM and ionic concentration determine the water quality [12, 13, 43]. The mixing process influences the floc formation and subsequent separation [13, 43, 45].

Zhang et al. (2022) studied the impact of water chemical conditions on PS NP (500 nm) removal by CFS, especially focusing on the pH and the presence of humic acid (HA, a NOM fraction) [3]. The solution pH influences the hydrolysis of the coagulant, the floc properties and the particle surface charge [3, 13]. Each coagulant has its optimal coagulation pH, which is why the water is sometimes pretreated by adding acids (HCl) or bases (NaOH) [12, 43]. Zhang et al. (2022) screened pH values between 6 and 9 to cover most wastewater scenarios and concluded that the higher pH ranges are more efficient for NP removal with PAC. Small and loose flocs were formed during the experiments with pH 6.0 and 7.0, these flocs did not adsorb to or trap the similar small-sized NPs. Observed R% were below 35 %. The efficiency significantly increased at pH 8.0 (90.7 %) and 9.0 (93.8 %) because the formed flocs were bigger (853.2 nm and 2276 nm versus ~ 600 nm) and able to entrap the NPs [3].

The concentration and characteristics of the (target) impurities in water influence the process, because the functional groups, MW and surface charges are important for the intermolecular interactions behind CF [12, 43]. By gradually increasing the HA concentration (5-20 mg/L) Zhang et al. (2022) revealed that HA generally reduces the removal efficiency of PS NPs by 6.7 %. The presence of HA increased the NP stability by adsorbing onto the particle's surface, inhibiting aggregation. However, higher HA concentrations facilitated more and denser flocs by adsorption to the flocs and by bridging different flocs with one another. This suggests competitive adsorption between HA and NPs [3]. Inorganic coagulants tend to form smaller flocs when the water contains mainly inorganic particles than when the water is rich in NOM. This can be attributed to the high MW of some NOM components, which results in a bigger floc size [3, 43].

Rapid initial mixing is crucial when using metal salts because the reaction sequence happens quickly (10^{-5} seconds) [12, 44, 45]. Initial mixing efficiency is especially important when the primary goal is to reduce the particle surface charge through charge neutralisation, which was the mechanism shown to be involved in all NP studies so far (Table 1) [2, 12]. After the rapid initial mixing, a more gentle mixing phase is needed to introduce collision between particles and to create flocs [44]. Since Abi Farraj et al. (2023) describe macro-flocculation as the major flocculation mechanism involved in NP removal [25] the mixing is important to obtain flocs that can be removed through sedimentation, (sand) filtration, flotation, or a combination of these methods [12, 43, 45].

Table 1: Overview of coagulant (doses), particle information, experimental information and identified mechanisms in different MP/NP studies.

Coagulant	Coagulant Dosage	Plastic Polymer	Particle Size	Particle Concentration	Flocculants or Coagulant Aids and Dosage	Removal Efficiency [%]	Time [min]	Mechanism
Microplastics (< 5 mm to > 0.1 µm)								
Alum [2]	2.73 mg Al/L	PE	15 µm	500 MPs/L	PAM: 0.3 mg/L	82	8	Combination of electrostatic interactions, hydrogen bonding, and bridging-like phenomena (= charge neutralisation, polymer bridging)
		PS	140 µm			84		
		PEST	14 × 581 µm			99		
AlCl$_3$·6H$_2$O [2]	5 mL	PE	d < 500 µm	0.1 g/L	N.A.	12.65	45	Combination of charge neutralisation, sweep flocculation, and floc cake layer formation
			500 < d < 1000 µm			10		
			1000 < d < 2000 µm			8.25		
			2000 < d < 5000 µm			8.23		
AlCl$_3$·6H$_2$O [46]	14.64 mg/L	PE	-	-	N.A.	96.10	-	-
FeCl$_3$·6H$_2$O [2]	2 mmol/L 112 mg/L	PE	d<500 µm	0.1 g/L	N.A.	<15	45	Sweep flocculation
			500<d<1000 µm		Cationic PAM: 15 mg/L	58		
			1000<d<2000 µm		Anionic PAM: 15 mg/L	90.91		
FeCl$_3$·6H$_2$O [2]	13.06 mg/L	PE	-	-	N.A.	70.56	-	-
FeCl$_3$ [2]	90 mg/L	PS	< 500 µm	500 mg/L	N.A.	63	46	Charge neutralisation, polymer bridging, and sweep flocculation
PAC [2]	90 mg/L	PS	<500 µm	500 mg/L	N.A.	77.83	46	Charge neutralisation, polymer bridging, and sweep flocculation
		PE				29.70		
		PE				10		
PAC [2]	20 mg/L	PET	100–400 µm	100 mg/L	N.A.	35.50	46	Combination of polymer bridging, sweep flocculation, and double-layer compression effect
					PAM: 5 mg/L	44.47		
					PAM: 100 mg/L	79.35		
Nanoplastics (< 0.1 µm or < 100 nm)								
AlCl$_3$ [2]	10 mg/L	PS-COOH	50 nm	50 mg/L	N.A.	96.6	101.5	Combination of electrostatic adsorption and intermolecular interactions (= charge neutralisation, polymer bridging)
FeCl$_3$ [2]	10 mg/L	PS-COOH	50 nm	50 mg/L	N.A.	95.8	101.5	Combination of electrostatic adsorption and intermolecular interactions (= charge neutralisation, polymer bridging)
PAC [3]	0.4 g/L	PS	50 nm	-	N.A.	85.6	45	Combined effects of sweeping flocculation, charge neutralisation, and affinity capacity
			100 nm			86.3		
			500 nm			98.5		
			1000 nm			89.3		

- = unknown/not tested for, N.A. = not applicable, d = diameter

Chapter 3
Materials & Methods

3.1. Survey of Dutch drinking water companies

In the Netherlands, DW is produced from groundwater (GW, 55 %), (dune infiltrated) surface water (SW, 40 %) and riverbank filtrate (RBF, 5 %) by ten drinking water companies (DWCs) (Figure 3). A survey was sent to the six DWCs that use SW at one of their production sites, to gain insight into the CFS protocol currently used by these companies. Questions revolved around the (quality of the) water source, the complete treatment train, the coagulation process, the chemicals and the water quality post-coagulation. Data from four companies (encircled in Figure 3) was collected and filtered to choose appropriate experimental conditions (Table 2). Appendix A gives an overview of all the questions and answers.

Figure 3: Map of Dutch drinking water companies with their distribution areas, sources, intake points and extracted water quantities (2018) [1]. Grondwater = groundwater, oevergrondwater = riverbank filtrate, infiltratie en natuurlijk duinwater = infiltrated and natural dune water, oppervlaktewater = surface water, noodinnamepunt = emergency extraction point, transport vanuit externe winning = transport from external extraction. Encircled the companies that provided data for this research.

Waterbedrijf Groningen, Evides and Waternet use CFS followed by RSF, while Dunea uses CFS followed by RSF. Since three out of four companies include the sedimentation step, this study focussed on CFS. The reported source turbidity was used as a guideline to select SW with a similar turbidity. Schie (canal) water was sampled at different locations to find the right turbidity. The pH of the selected SW matched the pH reported by the DWCs. This water was used to determine the theoretical coagulant dose. The experimental temperature was in range with the reported temperatures but higher than the average values. Experiments were done at room temperature in the TU Delft Waterlab because the water temperature could not be controlled during the experiment. Next, the survey helped select the most relevant coagulants and gave an indication of the doses used in practice. Flocculants were not considered for this research, since not all DWCs use these and they are only used in winter. pH adjustments were not systematically done, but NaOH and HCl were considered where needed. The final turbidity was one of the parameters considered to compare the efficiency of the experiments to practice.

Table 2: Data selected from the questionnaire to determine the experimental conditions.

	Waternet	Dunea	Evides	Waterbedrijf Groningen	Experimental conditions
Coagulation and floc separation steps	CFS + RSF	Coagulation + RSF	CFS + RSF	CFS + RSF	CFS
Source turbidity [NTU]	8.1	10.9	0.7-5.5, avg. 2.0	1-20.1, avg. 6	7.5 ± 1
Starting pH [-]	8.1	8-8.5	7.9-9.3, avg. 8.7	7.6-8.6, avg. 7.9	8 ± 0.5
Temperature [°C]	14.8	4-15, avg. 13.5	2.6-23.5, avg. 12.6	2.4-24.1, avg. 12.7	19 ± 1
Coagulant type	FeCl₃	FeCl₃	FeCl₃	PAC Sachtoklar	FeCl₃, AlCl₃, PAC
Coagulant dose	2.7 mg Fe/L	0.2-1 mg Fe/L	5 mg Fe/L	5-9 mg Al/L	Theoretical & Practical dose
Flocculant	N.A.	N.A.	Wisprofloc N (winter)	Wisprofloc N (winter)	N.A.
pH adjustments	N.A.	N.A.	NaOH before distribution	HCl during and after CFS	NaOH, HCl
Final turbidity [NTU]	-	0.7-1	0.4	0.2-0.6	Variable

CFS = coagulation-flocculation-sedimentation, RSF = rapid sand filtration, N.A. = not applicable, - = unknown

3.2. Chemicals

Based on the answers from the questionnaire and literature, three inorganic coagulants were selected for this research: iron(III)chloride about 40% (FeCl₃, VWR® BDH® Chemicals, CAS: 7705-08-0), anhydrous granular aluminium chloride (AlCl₃, Alfa Aesar GmbH & Co KG, CAS: 7446-70-0) and Sachtoklar® polyaluminium chloride (provided by Drinkwaterbedrijf Groningen, CAS: 39290-78-3). Working solutions were prepared by diluting liquid stock FeCl₃ and dissolving granular AlCl₃ in MiliQ water [12]. PAC was used in undiluted form, to ensure the coagulant stability [12]. The coagulant concentration and the concentration of the active component (Fe or Al) were calculated with Equation 1 and Equation 2 respectively. The concentration of the active component in the working solutions was verified with ICP-OES (procedure explained in section 3.5.3). The density of the solution was verified by calibrating a micropipette and weighing 1 mL of the stock solution on an AT261 DeltaRange® (©METTLER TOLEDO) analytical balance. The coagulant characterisation is explained more in-depth in Appendix E.

Equation 1: Coagulant concentration

$$C_{coagulant}\left(\frac{g\ liquid\ coagulant}{L}\right) = \frac{\%Fe\ or\ \%Al * \rho_{coagulant}\left(\frac{g}{mL}\right)*MW_{coagulant}\left(\frac{g}{mol}\right)}{MW_{Al\ or\ Fe}\left(\frac{g}{mol}\right)} * \frac{100\ mL}{1\ L}$$

Equation 2: Concentration of the active ingredient

$$C_{active\ ingredient}\left(\frac{gAl\ or\ gFe}{L}\right) = C_{coagulant} * \%Fe\ or\ \%Al * \frac{MW_{Al\ or\ Fe}\left(\frac{g}{mol}\right)}{MW_{coagulant}\left(\frac{g}{mol}\right)}$$

$$= (\%Fe\ or\ \%Al)^2 * \rho_{coagulant}\left(\frac{g}{mL}\right) * \frac{1000\ mL}{1\ L}$$

Three different sizes of PS NPs were used: microparticles based on PS 200 nm (Product: 69057), 500 nm (Product: 59769) and 1 μm (Product: 89904) were supplied by Sigma-Aldrich®. The NP stock solutions were diluted with MiliQ water to obtain a working solution of 100 mg/L. Nitric acid ROTIPURAN®Ultra 69 % (HNO₃, Carl Roth GmbH, CAS: 7697-37-2) was used to acidify the ICP-OES samples. Hydrochloric acid (HCl, Carl Roth GmbH, CAS: 7647-01-0) was used to determine the alkalinity and sodium hydroxide (NaOH, Sigma-Aldrich®, CAS: 1310-73-2) was used to basify the solution or samples where needed.

3.3. Water types

Three types of water were used for the experiments (overview Table 3): Schie water, NP spiked Schie water and NP spiked tap water. The Schie water and tap water were collected in big volumes to ensure that the composition was the same for all experiments. The water was stored at 5 °C. Schie water was used as the reference water in this study and to determine the theoretical optimal dose. Schie water is also spiked with 0.47 mg NP_{200}/L to accommodate a control experiment in a SW matrix.

Tap water was spiked with the different NPs in two different concentrations (scenarios). One concentration represents a turbidity of 7.5 NTU, because this is the turbidity of the Schie water used to determine the theoretical dose for turbidity removal in Schie water. The other concentration was adjusted to ensure a total particle surface area (SA) of 135 cm²/L (as in Farraj et al. (2024) 1.43 mg/L for 50 nm, 6.29 mg/L for 220 nm). This SA corresponds to a turbidity of 7.5 NTU for NP_{1000} (Appendix C). Choosing the SA corresponding to a turbidity of 7.5 NTU for NP_{500} or NP_{200} would result in turbidities higher than 7.5 NTU, which is why this was avoided. Additionally, the difference in NP mass concentration is highest between these two scenarios for NP_{200} (Appendix C) and 200 nm is the size closest to the most abundant NP size found in tap water (58-255 nm with concentrations 1.67 – 2.08 ug/L) [10], which is why the influence of different coagulants and doses was tested on NP_{200}. NP_{200}, NP_{500} and NP_{1000} were used to test the influence of NP size with PAC as coagulant.

Table 3: The turbidity, particle mass concentration, surface area and number for the different water types.

	Particle	Turbidity [NTU]	Concentration [mg/L]	Surface area [cm²/L]	Particle number
Schie water	-	7.5 ± 1	-	-	-
NP spiked tap water	NP_{1000}	7.5	2.36	135	4.29×10^9
	NP_{500}	7.5	2.1	240	3.06×10^{10}
		4.28	1.18	135	1.72×10^{10}
	NP_{200}	7.5	1.41	403	3.21×10^{11}
		2.78	0.47	135	1.07×10^{11}
NP spiked Schie water	NP_{200}	-	0.47	-	1.07×10^{11}

- = unknown

3.4. Jar tests: Experimental set-up and protocol

CFS can be studied, evaluated and optimized in the lab using bench-scale jar testing. Traditionally, these tests allow the screening of multiple coagulant types and dosages under different mixing conditions [12, 43]. The jar tests (JT) were used during this research to determine the NP R% achieved with three coagulants. Two different doses were used: the theoretical dose and the practical dose. The theoretical dose corresponds to a ζ-potential of -5 mV in Schie water, while the practical dose is determined from the questionnaire and literature. The theoretical dose was determined by dosing increasing coagulant doses to 0.5 L Schie water in 0.5 L Duran bottles on a LABINCO LD-746 magnetic stirrer plate. The solution was thoroughly stirred at 15 % for 1 minute after dosing and before taking a sample. The ζ-potential of each sample was measured to identify the coagulant dose that achieved a favourable ζ-potential of – 5 mV [49, 50]. Coagulant doses between 0-100 mg Al/L, 0-10 mg Al/L and 0-100 mg Fe/L were screened for $AlCl_3$, PAC and $FeCl_3$ respectively.

The theoretical dose was used in JTs performed in the JLT6 Flocculation Tester (VELP® Scientifica) filled with 600 mL water. Additionally, lower practical doses, corresponding to the doses reported by the DWCs, were tested for $AlCl_3$ (3.4 mg Al/L) and $FeCl_3$ (5 mg Fe/L). The jars were placed in a water bath, about mid-point height to obtain a temperature of 19 ± 1 °C before starting [51]. Stirrer paddles (25 mm high, 75 mm wide and 1 mm thick) were positioned halfway through the water sample in 1000 mL tall glass beakers (jars) with a diameter of 105 mm. The stirring conditions were set to turbulent stirring at 120 RPM for 2 minutes, followed by slow flocculation at 30 RPM for 25 minutes [52]. Once the stirrers were lifted from the sample, the flocs were allowed to settle for 30 minutes (sedimentation) [3]. After the experiment, samples (90 mL) were taken at a depth of 2.5 cm from the liquid surface. Table 4 summarises the experimental procedure.

Table 4: Experimental procedure based on VELP® Scientifica.

Procedure actions	Comments	Stirrer settings	Time
Prepare & sample the water	Spike water with NPs, ensure a temperature of 19 °C	N.A.	N.A.
Prepare the jars	Fill jars with water (600 mL – amount of coagulant), position the stirrer in the middle and start mixing	120 RPM	N.A.
Coagulation - Rapid stirring	Coagulant dosing at the beginning	120 RPM	2 min.
Flocculation - Slow stirring	Facilitate floc formation	30 RPM	25 min.
Sedimentation - Static settling	Allow floc sedimentation	0 RPM	30 min.
Supernatant sampling	Sample 90 mL supernatant for analysis, at 2.5 cm below surface	N.A.	N.A.

- = unknown

3.5.   Sample analysis

3.5.1.   Removal efficiency: UV-VIS and Turbidity

The NP-containing samples were analysed in duplicate with the GENESYS 10S UV-VIS Spectrophotometer (Thermo Fisher Scientific) at a detection wavelength of 298 nm. This wavelength was found as the maximum absorption peak during a full wavelength scan [7]. Tap water was used as a blank. The absorbances were translated into NP concentrations with a particle-specific calibration curve (Appendix D) based on known NP_{1000}, NP_{500}, NP_{200} (0-3 mg/L) concentrations and the measured absorbance. The (calculated) concentrations were used to determine the NP R% (Equation 4).

All samples were analysed in duplicate with the 2100N Turbidimeter (HACH®) to determine turbidity R% (Equation 3). The turbidimeter is equipped with a white light source and a 90-degree light detector to measure turbidity in nephelometric turbidity units (NTU) [53, 54]. The StabCal® calibration set 0 to 4000 NTU (HACH®) was used to check the accuracy each time the turbidimeter was used. Arenas et al. (2022), Lapointe et al. (2020) and Abi Farraj et al. (2024) effectively used turbidity to determine NP R% with calibration curves [25, 33, 34]. Skaf et al. (2020) claim that turbidity is more sensitive than absorbance as an indicator for MP concentration in tap-water experiments [55]. The turbidity measurements were therefore also translated to NP concentrations using the particle-specific calibration curves (Appendix D). The particle R% was then determined by Equation 4.

Equation 3: Turbidity removal efficiency

$$Turbididty\ removal\ efficiency\ (\%) = \frac{NTU_0 - NTU_s}{NTU_0} * 100\%$$ with NTU_0 = initial turbidity [NTU]

NTU_s = supernatant turbidity [NTU]

Equation 4: Particle removal efficiency

$$Particle\ removal\ efficiency\ (\%) = \frac{C_0 - C_s}{C_0} * 100\%$$ with C_0 = initial particle concentration [mg/L]

C_s = supernatant particle concentration [mg/L]

3.5.2.   Particle stability: ζ-potential

The ζ-potential is used as a relative measure of the particle surface charge [12] and seen as a key parameter to evaluate the stability of particles in suspension. Efficient CF occurs at values between -5 and 5 mV [3, 56]. The ζ-potential was determined with the Zetasizer Nano ZS (Malvern Instruments Co. LTD) during the first stage of the research, and with the Litesizer DLS 700 (Anton Paar GmbH) after that. A folded capillary cell or omega cuvette is used for these measurements. Samples are injected into the cell with a syringe. Air bubbles need to be removed by tapping until they are dislodged. The ζ-potential is determined from the particle velocity, the applied electrical field, the sample velocity and the dielectric constant. The final values are based on a series of three measurements (100 runs) per sample [57, 58].

3.5.3. Residual coagulant concentration: ICP-OES

The 5800 ICP-OES (Agilent) was used to determine the residual coagulant concentration. This parameter is often overlooked, because the focus of coagulation studies mostly goes to monitoring the residual target pollutant. There are, however, legal threshold concentrations for both Al and Fe in finished DW (200 μg/L) and it provides info on whether the DWTP/techniques function properly [13, 59, 60]. CHROMAFIL®Xtra PES-20/25 disposable syringe filters (Macherey-Nagel GmbH & Co. KG) were used in combination with BD Luer-Lok™ Syringes (BD Plastipak™) to filter the samples. These samples were diluted with MiliQ water to ensure Al- and Fe-concentrations between 0.025 and 50 mg/L and acidified with 1 % (v/v) HNO_3 to keep the metals in solution. The electrons in the sample take up thermal energy and reach a higher excited state. Eventually, electrons drop back to their ground level and energy is liberated as light (photons) at a specific emission spectrum. The signal intensity is measured with the built-in spectrometer and translated into a concentration with the calibration values. The measurements are done at an axial wavelength of 237.312/308.215/396.152 nm and 234.350/238.204/259.940 nm for Al and Fe respectively. For Fe, the samples are also analysed at a radial wavelength of 240.489 nm [61]. The average of these results gives the residual concentration.

3.5.4. Alkalinity: End-point titration

Alkalinity is defined as the capacity of water to neutralise hydrogen ions or acids [62, 63]. Coagulants react with water to form hydroxide precipitates, and the released hydrogen ions react with the alkalinity of the water. The alkalinity acts as a buffer to ensure the pH stays within a range where the coagulant is effective, and where complete coagulation can occur [62]. The 702 SM Titrino titrator (Metrohm AG) was used to determine alkalinity (1/sample). The titrator is equipped with a burette and a pH electrode. Both need to be submerged centrally into the sample (40 mL) while the sample is being mixed on the magnetic stirrer plate. The Set End-point titration option was used to titrate to a pH of 4.3. The maximum and minimum titration rates were set to 10.0 mL/min and 25 μL/min. 0.1 M HCl was used to obtain the end-point pH, and the added volume was used in Equation 5 to obtain the sample alkalinity. Samples were alkalised with 0.5 M NaOH when the pH was lower than the end-point pH. The maximum titration rate for these samples was adjusted to 5.0 mL/min, but the other parameters were kept the same. Later during the research, the titrations had to be done with a burette, because the Titrino broke down.

Equation 5: Alkalinity determination by acid-titration

$$Alkalinity \left(\frac{CaCO3}{L}\right) = \frac{V_{acid}*N*50\ 000}{V_{sample}}$$ with V_{acid} = volume of acid to reach pH 4.3 [mL]

N = normality of the acid [eq/mol] (Equation 6)
V_{sample} = volume of the sample [mL]

Equation 6: Normality of a solution

$$Normality \left(\frac{eq}{mol}\right) = M * \#H$$ with M = molarity [mol/L]

$\#H$ = number of hydrogen exchanged in reaction [eq/mol]

Chapter 4
Results

4.1.   Theoretical and practical coagulant dose for turbidity removal in Schie water

The theoretical dose to remove turbidity from Schie water (7.6 ± 0.28 NTU) was defined as the coagulant dose corresponding to a ζ-potential of -5 mV for this study. Dose screening on the magnetic stirrer plate resulted in theoretical optimum doses of 65.2 mg Fe/L, 14.3 mg Al/L and 8.8 mg Al/L for $FeCl_3$, $AlCl_3$ and PAC respectively. Linear regression equations were generated to determine these doses (y = -5 mV). Figure 4 shows the residual turbidity and the ζ-potential for the screened doses, together with the linear regression equations and the trendline reliability (R^2). The residual turbidity only gives a first impression of the settleability of the flocs, because the settling conditions in the 0.5 L Duran bottles are not representative of the actual JT settling conditions [51].
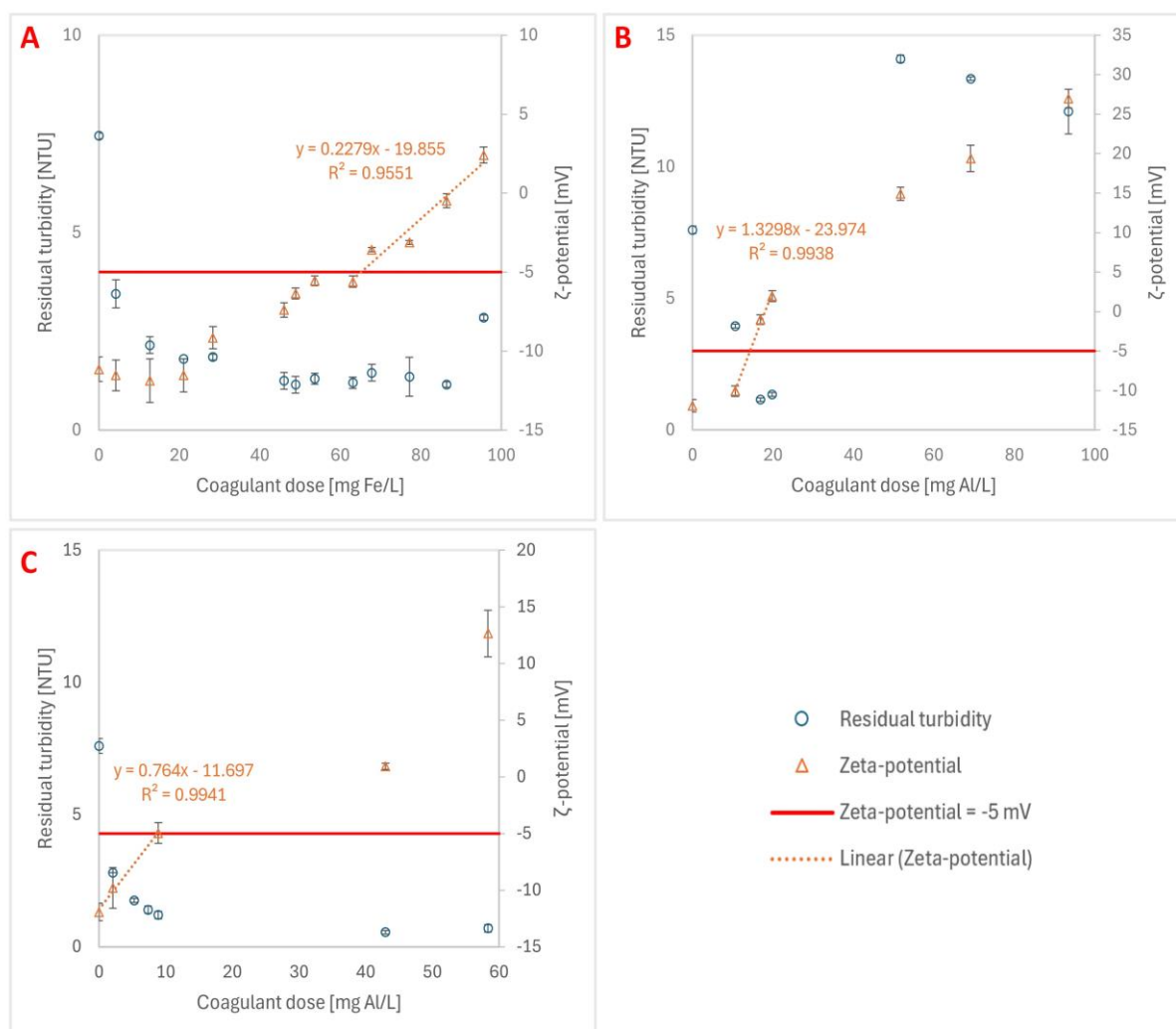
Figure 4: Screened coagulant doses, corresponding residual turbidity and ζ-potential for $FelCl_3$ (A), $AlCl_3$ (B) and PAC (C). Results are presented as a mean with corresponding minimum and maximum values obtained from 2 measurements for turbidity and 3 measurements for ζ-potential.

The questionnaire (Appendix A) revealed that practical doses in Dutch DWCs are lower than the theoretical optimum dose determined via ζ-potential measurements. Moreover, none of the DWCs reported measuring or using ζ-potential to determine the practical dose. In practice, the floc properties and the final turbidity are more important. Floc properties influence the floc separation efficiency [43, 45] and the final turbidity needs to meet the finished DW requirements (≤ 1 NTU in the Netherlands) [59]. Dunea, Waternet and Evides use $FeCl_3$ at doses of 0.2-1, 2.7 and 5 mg Fe/L respectively, so 5 mg Fe/L was selected to study the efficiency of this practical dose for NP removal. $AlCl_3$ is less commonly used in DWTPs, so the practical dose was calculated based on a reference $Al_2(SO_4)_3$-dose used from a DWTP in Detroit (20 ppm) [21]. This was converted to mg Al/L with a conversion curve (Appendix F) [13], resulting in a practical $AlCl_3$ dose of 3.15 mg Al/L. No lower dose was tested for PAC, because the tested theoretical dose (8.8 mg Al/L) was already within the practical range used by Drinkwaterbedrijf Groningen (5-9 mg Al/L). The results from the experiment with Schie water serve as a reference and used to compare the efficiency of the CFS process for 'normal' particles with the CFS process efficiency for NP particles. Figure 6 visualises all the results from this set of experiments. The summary of all R% and water quality parameters can be found in Appendix G.

4.1.1. $FeCl_3$

The theoretical optimum $FeCl_3$ dose and the practical dose achieved a turbidity R% of 84.35 % and 78.70 % respectively. The ζ-potential measurements show that the theoretical dose is more efficient in destabilising the particles (Table 5). Both doses resulted in good floc formation, but visually the flocs look smaller and less dense for the practical dose than the theoretical dose. Most flocs settled well after 30 minutes, but some are still floating in the supernatant for the practical dose. The supernatant is therefore less clear than achieved with the theoretical optimal dose. The produced amount of sludge is visually less in the experiments with the practical dose, which is favourable for the DWCs [13, 21]. These observations can be seen in Figure 5. The alkalinity drop is similar for both doses (~ 40 mg $CaCO_3$/L), while the pH drop is smaller for the practical dose (7.72) than the theoretical dose (6.41). The legal limit of Fe in finished DW is 200 µg Fe/L [13] and the residual coagulant concentrations were well below this limit for both doses, but higher for the practical dose than the theoretical one.

4.1.2. $AlCl_3$

Similarly to the findings for $FeCl_3$, adding the theoretical optimum $AlCl_3$ dose to Schie water resulted in good floc formation and a clear supernatant. The turbidity was reduced by 85.03 %. The operational dose was still effective in reducing turbidity, though less so than the optimum dose (80.14 %). Some flocs were left in the supernatant after 30 minutes (Figure 5). The ζ-potential measurements show that the theoretical dose is more efficient in destabilising the particles (Table 5). The theoretical dose reduced the initial alkalinity from 177 ± 10.43 mg $CaCO_3$/L to 49 mg $CaCO_3$/L and the pH from 7.84 to 6.37. The practical dose caused a similar alkalinity drop, but a smaller pH reduction (7.55). These observations align with the observations for $FeCl_3$. Similar to Fe, the legal limit of Al in finished DW is 200 µg Al/L [13]. This limit is slightly exceeded with the practical dose (0.25 mg Al/L), while the theoretical dose obeys the threshold.

4.1.3. PAC

The theoretical PAC dose corresponds to the practical dose and effectively destabilised the particles (Table 5), reducing the turbidity in Schie water by 87.76 %. This is the highest R% obtained between the three coagulants and the different doses. It was the only coagulant that obtained a turbidity lower than the guideline 1 NTU in finished DW (0.90 NTU). The questionnaire already suggested that PAC would be the most powerful coagulant when it comes to turbidity removal, since Drinkwaterbedrijf Groningen has the highest initial turbidity (0.1-30 NTU) but produced the CFS effluent with the lowest turbidity (0.2-0.6 NTU). The DWCs using $FeCl_3$ produce CFS effluents with turbidities between 0.4 and 1 NTU (Appendix A).

PAC only slightly decreased the alkalinity to 161 mg $CaCO_3$/L, and the pH to 7.18. Even for the lower practical coagulant doses, the drop in pH and alkalinity for the other coagulants is much bigger than the drop observed for PAC. Since PAC already contains polynuclear hydrolysis products, this coagulant does not require (as much) initial hydrolysis. The prehydrolysed PAC thus consumes less alkalinity and has a smaller impact on the final alkalinity and pH [13, 51]. On the contrary, the residual aluminium concentration was 0.27 mg Al/L, exceeding the legal threshold more than any other coagulant.
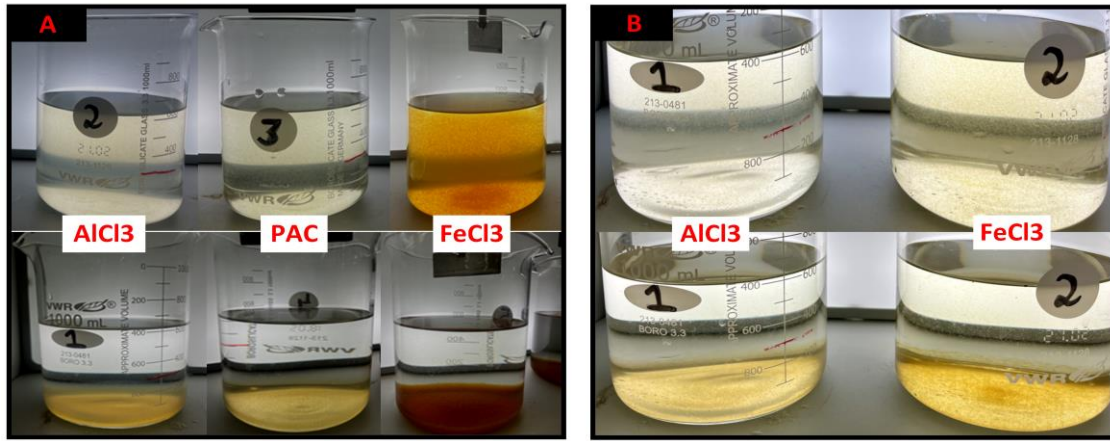
Figure 5: Flocs in Schie water before settling (top) and after 30 minutes of settling (bottom). Box A shows the jars with the theoretical optimum dose, box B shows the jars for the practical dose.
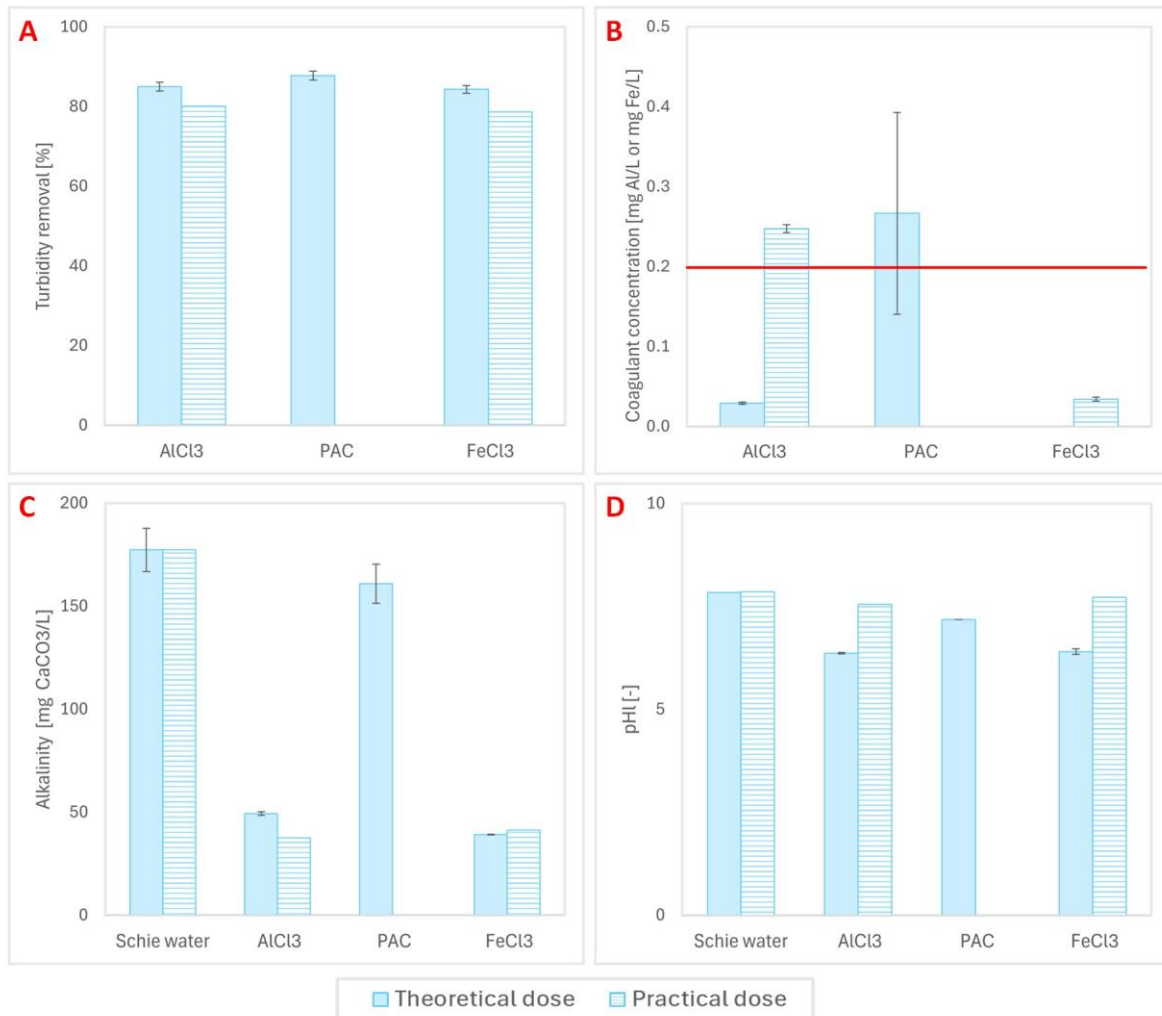
Figure 6: Turbidity removal efficiency (A) and residual coagulant concentration (B) for the different coagulants and doses. Graph C and D visualise the pH and alkalinity before and after the experiment. The error bars visualise the minimum and maximum observed in duplicate experiments for the theoretical doses. Only one dose was tested for PAC.

Table 5: ζ-potential values (particle stability) for the Schie reference experiments.

Experiment	Initial ζ (mV)	Supernatant ζ (mV)
$FeCl_3$ – optimum dose		-4.48 ± 1.8
$FeCl_3$ – practical dose		-11.2 ± 0.44
$AlCl_3$ – theoretical dose	-12.57 ± 0.81	-0.98 ± 0.73
$AlCl_3$ – practical dose		-9.87 ± 0.45
PAC – theoretical & practical dose		-4.95 ± 1.4

4.2. Nanoplastic removal: influence of coagulant type

In this set of experiments 65.2 mg Fe/L (FeCl$_3$), 14.3 mg Al/L (AlCl$_3$) and 8.8 mg Al/L (PAC) were individually dosed to tap water that was spiked with either 1.41 mg/L (turbidity scenario = 7.5 NTU) or 0.47 mg/L (SA scenario = 135 cm²/L) NP$_{200}$ (Appendix C). The turbidity of the tap water (0.26 ± 0.12 NTU) increased to 6.89 NTU and 3.01 NTU respectively. The tap water used to prepare the NP solutions had an alkalinity of 100 ± 1.61 mg CaCO$_3$/L and a pH of 7.39. The alkalinity and the pH of the water did not change much with the addition of the NPs. The starting alkalinity equalled 103 mg CaCO$_3$/L for the turbidity-based experiment and 100 ± 0.53 mg CaCO$_3$/L for the SA-based experiment. The starting pH was 7.51 and 7.55 respectively. The experiments were done in duplicate for AlCl$_3$ but were only done once for PAC and FeCl$_3$. The summary of all R% and water quality parameters can be found in Appendix G and they are visualised in Figure 8.

4.2.1. FeCl$_3$

The JT experiments were initially conducted without pH adjustments. The alkalinity dropped significantly, and the pH fell below 4.5, indicating insufficient buffer capacity. The 65.2 mg Fe/L did not facilitate any floc formation or turbidity removal after 30 minutes. After 24 hours, however, flocs had formed and settled (Figure 7). This reduced the turbidity by 92.76 % in the turbidity scenario and 68.79 % in the SA scenario, respectively corresponding to NP R% of 97.91 % and 79.79 %. The NP concentration and NP R% could not be confirmed with UV-VIS, because the supernatant still had an orange colour (caused by the coagulant) that influenced the UV-VIS measurements. Even though a settling time of 24 hours is not workable in practice, this observation is interesting to consider when looking at the mechanisms at play during NP removal. Without charge neutralisation, sweep flocculation can still facilitate NP removal.

The performance of FeCl$_3$ was much better in a repeated experiment with pH adjustments to pH 7.2. The coagulant was added to the jars with a predefined volume (0.42 mL/L) of 0.5 M NaOH to ensure sufficient buffer capacity for the initial hydrolysis. The final pH values were more stable (> 6.2), but the supernatant alkalinity remained low (< 10 mg CaCO$_3$/L). Turbidity was reduced by 96.44 % and 91.86 % for the turbidity and SA scenario respectively. The residual turbidity values were lower than the initial tap water turbidity, indicating NP R% higher than 100 %. NP concentration could not be confirmed with UV-VIS due to residual concentrations being below the limit of detection (LOD). The ζ-potential measurements (Table 6) indicated successful particle destabilisation for both the turbidity and the SA scenario, supporting the finding of high R%. The residual Fe concentration was within the legal limits for both scenarios.

4.2.2. AlCl$_3$

Without pH adjustment, dosing 14.3 mg Al/L AlCl$_3$ caused a drop in alkalinity and pH like FeCl$_3$. No flocs were formed and no turbidity removal was observed after 30 minutes. Some flocs had formed and settled after 24 hours, but less than for FeCl$_3$ (Figure 7). The supernatant was still turbid, and turbidity reduction only occurred in the turbidity scenario (34.08 %). The NP R% equalled 35.97 %. UV-VIS could not be used to determine the NP R%, because the residual coagulant concentration interfered with the measurements (cloudy solution). The ICP-OES measurements confirm that almost the entire dose of AlCl$_3$ remained in the supernatant (> 13.5 mg AL/L), indicating poor reaction with the particles.

The repeated experiment with pH adjustments obtained better results. The final pH was closer to the initial values (> 6.8) but again, the supernatant alkalinity turned out way lower than the initial alkalinity. The observed turbidity R% were lower than observed for FeCl$_3$, but still high (> 87.5 %). The residual turbidities were below 1 NTU in both scenarios. The corresponding NP R% equalled 95.3 % and 100.95 % for the turbidity and SA scenario respectively. The NP R% could not be confirmed with UV-VIS for any of the samples, because the absorbance was close to or below the LOD (~ 0.05 mg/L). The ζ-potential measurements confirmed effective particle destabilisation (Table 6), and the ICP-OES measurements confirmed that the coagulant was removed together with the particles. The residual Al concentration was way lower than the dosed 14.3 mg Al/L but still exceeded the legal threshold in the turbidity scenario (0.66 mg Al/L). In the SA scenario, the residual concentration was below the threshold (0.07 mg Al/L).

4.2.3. PAC

PAC is the only coagulant that did not require pH adjustments for efficient turbidity and NP removal. Dosing 8.8 mg Al/L PAC resulted in good floc formation and a clear supernatant. The turbidity was reduced by 94.01 % and 93.45 % in the turbidity and SA scenario respectively. The corresponding NP R% were 99.23 % and over 100 %, respectively. As for the other coagulants, NP concentration could not be confirmed with UV-VIS due to residual concentrations being below the limit of detection (LOD). The ζ-potential measurements again confirmed successful particle destabilisation in both scenarios (Table 6). PAC had a smaller impact on alkalinity and pH compared to $AlCl_3$ and $FeCl_3$. In both scenarios, the pH stayed close to 7 and the alkalinity was reduced to 57 mg $CaCO_3$/L indicating that the initial hydrolysis requires less buffer capacity. This is as expected because PAC, as a pre-hydrolysed metal salt, has different mechanisms than the other two inorganic coagulants [12, 13]. The residual Al concentration after PAC treatment was well below the legal limits and lower than the Al residuals found for experiments with $AlCl_3$.
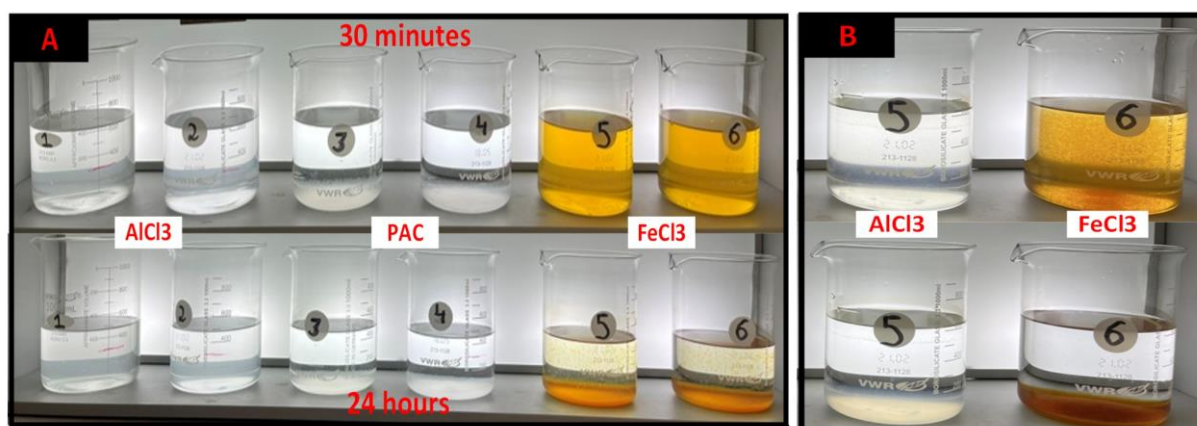
Figure 7: Box A shows the jars from the experiment without pH adjustment after 30 minutes (top) and 24 hours (bottom) for AlCl3 (left), PAC (middle), FeCl3 (right). Box B shows the jars from the repeated experiment for AlCl3 (left) and FeCl3 (right) with pH adjustments.

4.3. Nanoplastic removal: theoretical versus practical dose

4.3.1. FeCl$_3$

The previous experiment was repeated with the practical doses of $AlCl_3$ and $FeCl_3$ to assess the influence of the coagulant dose on NP removal efficiencies. The experiments with the practical dose did not require any pH adjustments to produce flocs. The practical dose caused a comparable drop in alkalinity (~ 10 mg $CaCO_3$/L) than the theoretical dose for both the turbidity and the SA scenario. The pH values are difficult to compare between the two doses, since the final pH of the experiments with the theoretical dose is influenced by the pH adjustments.

In the turbidity scenario, the obtained turbidity R% was in line with observations for the higher theoretical dose (93.49 %). Compared to the turbidity R% achieved with the theoretical dose, the CFS was less efficient for the SA scenario (55.69 %). The NP R% for the turbidity-based experiment was 98.68 % and 94.86 % calculated from the turbidity and UV-VIS measurements respectively. For the SA-based experiment, the NP R% was 64.59 % (turbidity) and 58.82 % (UV-VIS). The ζ-potential measurements indicated effective particle destabilisation for both NP scenarios (Table 6), though the ζ-potential reduction was smaller compared to the theoretical dose. Both the turbidity-based and SA-based supernatants had low residual Fe concentrations well within the legal threshold.

4.3.2. AlCl$_3$

Similar to the practical $FeCl_3$ dose, no pH adjustments were necessary for effective CFS with the practical $AlCl_3$ dose. The supernatant alkalinity values align with those found for the theoretical dose (~ 10 mg $CaCO_3$/L). The final pH in the turbidity scenario was 6.95, which is more acidic than with the theoretical dose; however, direct comparison is difficult due to additional buffer capacity in other experiments. In the SA scenario, the final pH was slightly higher at 7.12.

The obtained turbidity R% equalled 89.95 % and 51.74 % for the turbidity and SA scenario respectively. Again, the R% for the turbidity scenario is in line with the observations for the theoretical dose, while the R% is lower for the SA scenario. The NP R% calculated from UV-VIS data were 94.86 % and 56.99 %, which closely matched those derived from turbidity data (95.93 % and 57.89 %). Although the ζ-potential values indicate less charge reduction than with the optimum dose, the final values are still within the range considered optimal for CF (-5 to 5 mV) [56]. The residual Al concentration remained below threshold values in both scenarios. The SA-based experiment showed a comparable concentration to the theoretical dose experiment, while the turbidity-based supernatant had a much lower residual concentration.

Table 6: ζ-potential values (particle stability) for the experiments with NP200.

Experiment	T scenario Initial ζ [mV]	T scenario Supernatant ζ [mV]	SA scenario Initial ζ [mV]	SA scenario Supernatant ζ [mV]
$FeCl_3$ – theoretical dose		-3.33 ± 0.47		0.03 ± 0.35
$FeCl_3$ – practical dose		-4.43 ± 0.35		-1.13 ± 0.86
$AlCl_3$ – theoretical dose	-14.23 ± 0.32	5.40 ± 2.52	-10.10 ± 0.79	0.07 ± 0.06
$AlCl_3$ – practical dose		-0.53 ± 0.70		-0.47 ± 0.21
PAC – theoretical & practical dose		-1.57 ± 1.61		-0.37 ± 0.38

T = turbidity SA = surface area
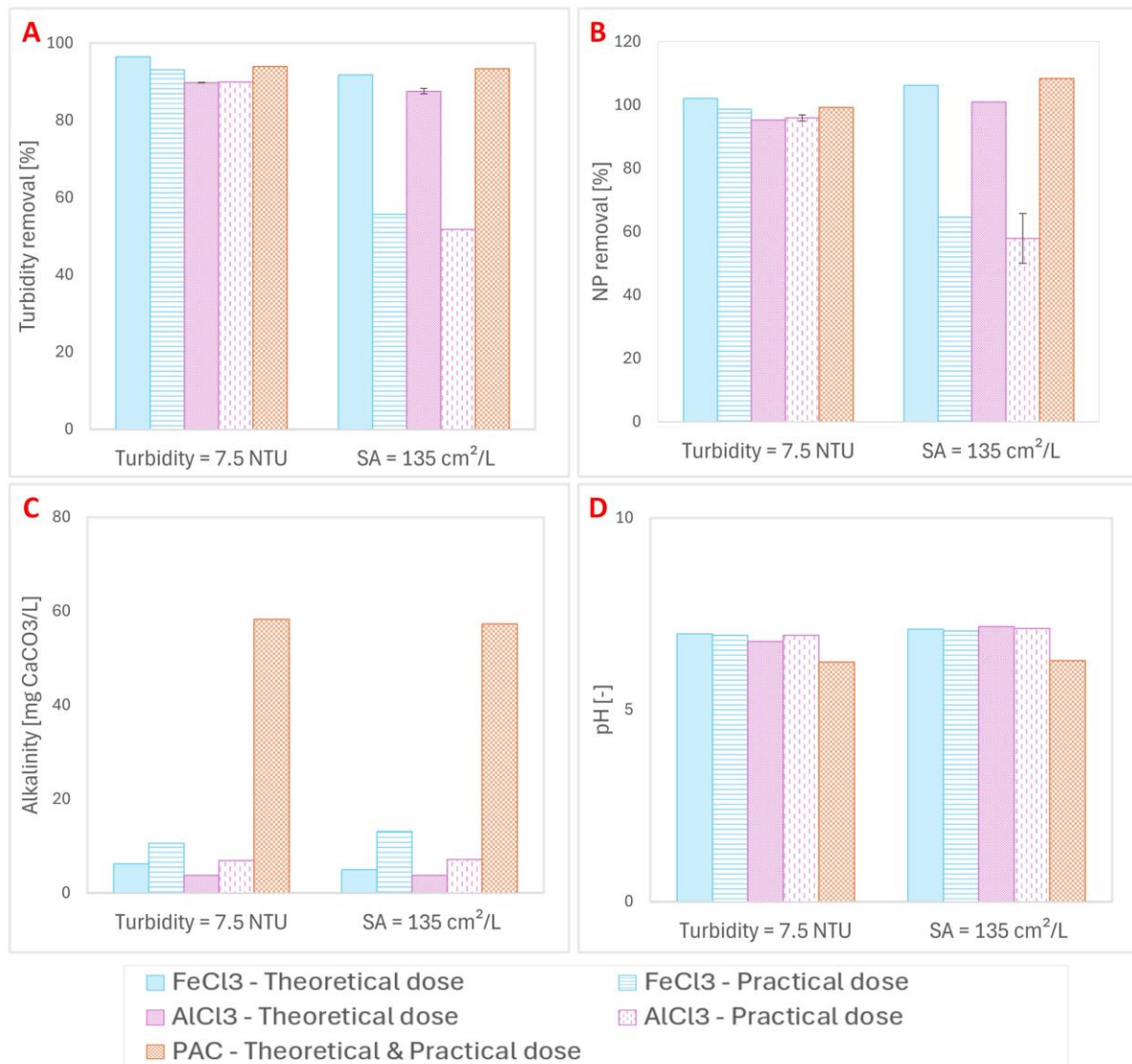
Figure 8: Turbidity removal efficiency (A) and NP removal efficiency (B) for the different coagulants and doses, aswell as final alkalinity (C) and pH (D) in the supernatants. Only one dose was tested for PAC. Experiments with the theoretical $AlCl_3$ dose were done in duplicate, minimum and maximum values are visualised with error bars.

4.4.   Nanoplastic removal: influence of nanoplastic size

The influence of the NP size on the R% was investigated for PAC only, since the previously described results show that this is the most efficient coagulant considering both dosage and R%. Additionally, PAC is less temperature-dependent than $AlCl_3$ and $FeCl_3$ [12, 43, 45]. Since the temperature of the lab experiments was higher (19 ± 1 °C) than the mean operational temperature in Dutch DWCs (12.5-15 °C, Appendix A) the PAC results might be most representative of the industrial setting. The summary of all R% and water quality parameters can be found in Appendix G and are visualised in Figure 9.

As for the previously described experiments, two NP scenarios were tested. Different concentrations of different sizes were dosed to tap water to prepare the experimental solution (Chapter 3, Table 3). The turbidity scenario targeted a starting turbidity of 7.5 NTU for all NP sizes, while the starting turbidities equalled 4.49 and 2.9 NTU for the SA scenario of NP_{500} and NP_{200}. The two scenarios are equal for NP_{1000}. The addition of any of the NP sizes or concentrations did not influence the initial tap water alkalinity and/or pH. The starting alkalinity for all these experiments was thus 100 $mgCaCO_3$/L, while the starting pH equalled 7.39.

In the turbidity-based experiments, the turbidity R% was highest for the largest NP size, NP_{1000} (97.22 %). The R% slightly decreased as the particle size decreased, e.g. 95.43 % and 94.01 % for NP_{500} and NP_{200} respectively. The residual turbidity was lower than 1 NTU in all supernatants. The NP concentrations could not be determined with UV-VIS for any of the samples, because the absorbance was below the LOD (~ 0.05 mg/L). However, the turbidity values were translated to NP concentrations and showed reductions from 2.32 to 0.02 mg/L, from 2.15 mg/L to 0.06 mg/L and from 1.43 mg/L to 0.01 mg/L for NP_{1000}, NP_{500} and NP_{200} respectively. These values correspond to NP R% of 99.34 %, 95.92 % and 99.23 % respectively, indicating a difference with the observations for the turbidity R%. The experiments started with ζ-potential values between - 14.23 and -19.00 mV and were reduced to values between -0.58 and -1.80 mV, confirming effective CF and supporting the high R% that were found. Both alkalinity and pH dropped uniformly across all NP sizes. Supernatant alkalinity was between 55-58 mg $CaCO_3$/L, and the supernatant pH values were all in the range of 6.2-6.4. The residual Al concentration was well below the legal threshold for all the NP sizes. The dosed 8.8 mg Al/L thus efficiently reacted with the particles in solution and precipitated with the flocs, leaving around 0.05 mg Al/L in the supernatant after 30 minutes. The alkalinity, pH and residual coagulant suggest no operational difference for the different NP sizes.

In the SA-based experiment, the R% were similar for NP_{500} (93.65 %) and NP_{200} (93.45 %), but lower than those for NP_{1000} and the NP_{500} and NP_{200} efficiencies in the turbidity scenario. The NP_{500} concentration went from 1.24 mg/L to 0.04 mg/L (91.99 %) and all the NP_{200} particles were removed. Again, the LOD of the UV-VIS technique did not allow to verify the NP concentrations. The initial ζ-potential values of the SA experiments were lower than for the turbidity-based experiments, and the supernatant measurements show slightly better destabilisation Similar to the turbidity-based scenario, the alkalinity and pH decreased uniformly for the three NP sizes and the residual Al concentration obeyed the legal thresholds.
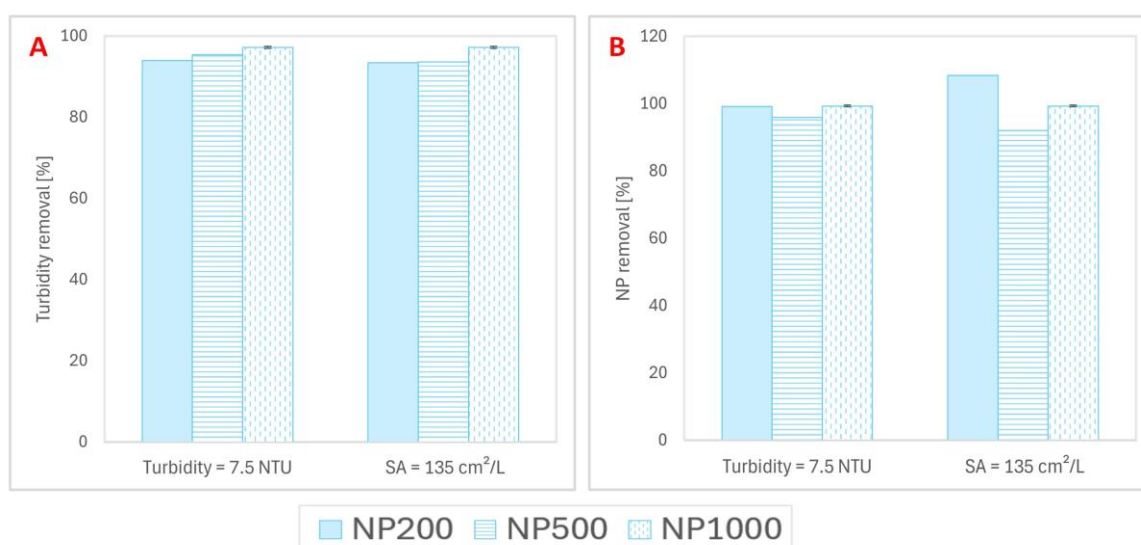
Figure 9: Turbidity removal efficiency (A) and NP removal efficiency (B) for the different NP sizes. Experiments were done with PAC. The error bars represent the minimum and maximum value observed in a duplicate experiment (only for NP1000).

Table 7: ζ-potential values (particle stability) for the PAC experiments with NP_{200}, NP_{500} and NP_{1000}.

Experiment	Initial ζ (mV)	Supernatant ζ (mV)
NP_{200} – Turbidity	-14.23 ± 0.32	-1.57 ± 1.61
NP_{200} – Surface area	-10.10 ± 0.79	-0.37 ± 0.38
NP_{500} – Turbidity	-19.00 ± 0.33	-1.80 ± 1.97
NP_{500} – Surface area	-14.93 ± 1.22	-0.07 ± 0.06
NP_{1000} – Turbidity & surface area	-18.10 ± 0.67	-0.58 ± 1.04

4.5. Nanoplastic removal in Schie water

The section describes the results from the same type of experiments as before, but now with 0.47 mg NP_{200}/L in Schie water (SA scenario). The Schie water turbidity increased from 7.30 to 13.85 NTU after spiking the water. This did not influence the pH but seemed to affect the alkalinity (drop 177 ± 10.43 to 45 mg $CaCO_3$/L). However, the alkalinity values were determined with a manual titration instead of the Titrino (broken) and should therefore not be overanalysed. The ζ-potential measurements show a slight difference in particle stability in Schie water and Schie water spiked with NP_{200}, i.e. -12.57 ± 0.81 mV and − 9.47 ± 3.14 mV respectively. The standard deviation of the ζ-potential with the spiked solution is quite big and overlaps with the ζ-potential of the Schie water (Table 8).

These experiments with NP-spiked Schie water cannot be directly compared to the other experiments, because the starting turbidity is higher than the maximum 7.5 NTU used before. Additionally, there is no way to distinguish between the particles naturally present in Schie water and the spiked NPs. However, these experiments give a first indication of R% in a SW matrix instead of in tap water.

4.5.1. FeCl₃

The experiments for FeCl₃ were done with both the theoretical and the practical dose. The biggest difference compared to the experiments in tap water is that the experiments with the theoretical dose did not require any pH adjustments to facilitate efficient CFS. The theoretical dose of FeCl₃ reduced turbidity by 91.99 %. The practical dose was less efficient, obtaining a R% of 78.74 %. The ζ-potential measurements (Table 8) did not show much variation between the two doses (~ -11 mV), indicating that particle destabilisation was similar in both scenarios, despite the different R%. This confirms that sweep flocculation is more at play for the higher theoretical doses than the lower practical ones, as observed during the tap water experiments. The pH was more acidic for the supernatant produced with the theoretical dose (6.42) than with the practical dose (6.75). The final alkalinity was similar for both supernatants, which is comparable to the findings for experiments in tap water. Residual coagulant concentrations were well below the legal threshold for both FeCl₃ doses.

4.5.2. AlCl₃

As for FeCl₃, both the theoretical and practical dose were tested without pH adjustments. The difference between the turbidity R% obtained for the two doses is smaller than for FeCl₃, e.g. 86.79 % and 81.99 % for the theoretical and practical dose respectively. However, the final ζ-potential values (Table 8) do indicate a difference in particle stability. The value for the theoretical dose (-4.33 mV) falls within the optimal range for CF, while the practical dose destabilised the particles less (-11.37 mV). The final ζ-potential achieved with the practical dose is comparable to the values found for both FeCl₃ doses. As observed in previous experiments, the pH drop was bigger for the theoretical dose than the practical dose, comparable to what was observed for FeCl₃. The residual Al concentration was higher in the experiment with the practical dose (0.35 mg Al/L) than the theoretical dose (0.10 mg Al/L), exceeding the legal threshold of 0.2 mg Al/L.

4.5.3. PAC

PAC proved to be the most effective coagulant in terms of turbidity reduction (94.66 %, residual 0.74 NTU), although the supernatant ζ-potential (-9.73 mV) was not in the range of the values considered most optimal for CF and the values indicate less particle destabilisation than with the theoretical AlCl₃ dose (Table 8). In terms of alkalinity and pH, PAC caused a smaller reduction compared to the other two coagulants. The residual coagulant concentration for PAC was 0.21 mg Al/L, showing that even though the coagulant is highly effective in removing turbidity, it results in a residual concentration close to the regulatory limit for Al.

Table 8: ζ-potential values (particle stability) for the experiment with NP-spiked Schie water.

Experiment	Schie ζ [mV]	Experimental ζ [mV]	Supernatant ζ [mV]
FeCl$_3$ – theoretical dose			-11.37 ± 0.85
FeCl$_3$ – practical dose			-11.90 ± 0.25
AlCl$_3$ – theoretical dose	-12.57 ± 0.81	− 9.47 ± 3.14	-4.33 ± 0.31
AlCl$_3$ – practical dose			-11.37 ± 0.85
PAC – theoretical & practical dose			-9.73 ± 1.47
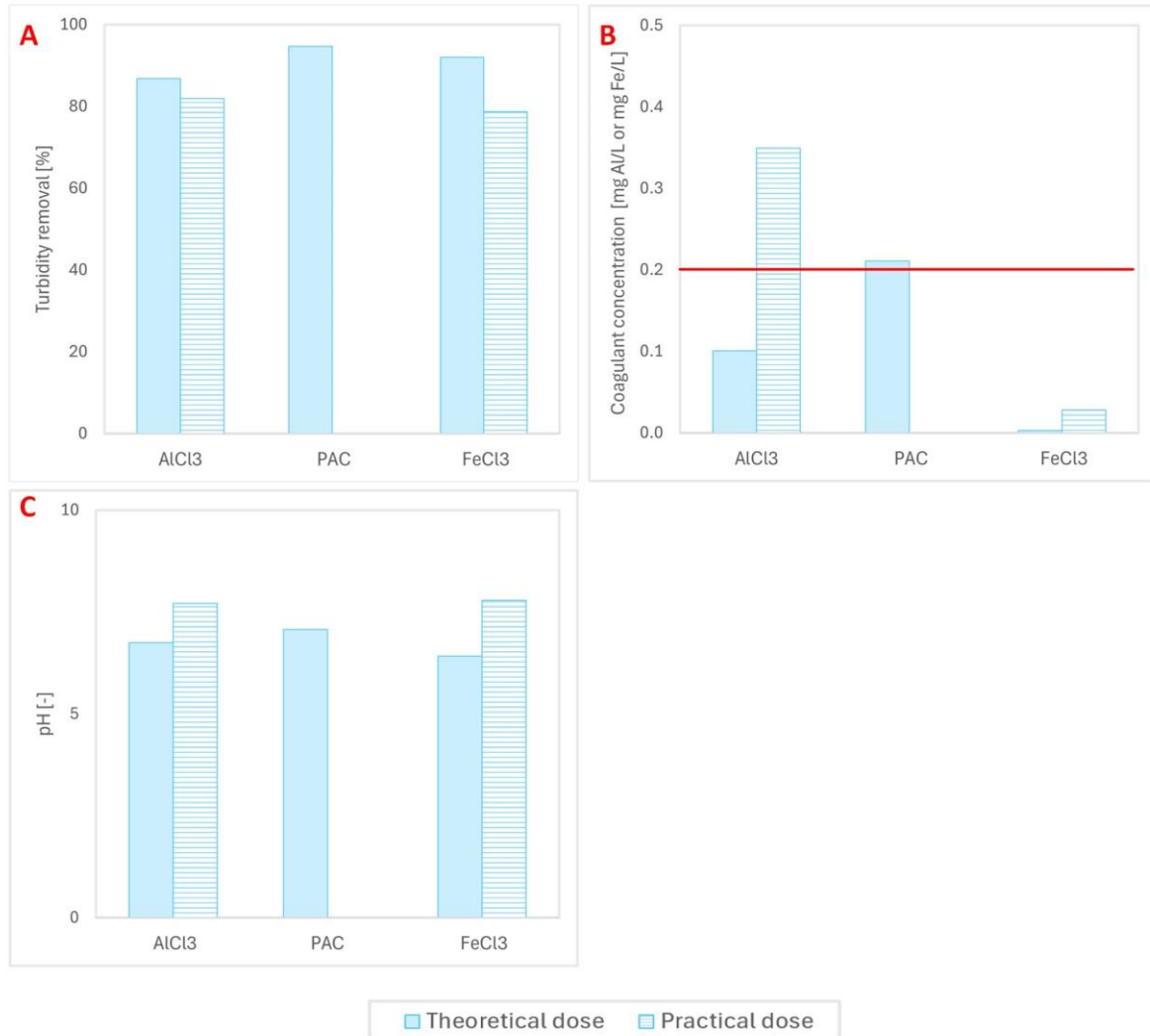
Figure 10: Graph A shows the turbidity removal efficiency. Graph B and C show residual coagulant concentration and pH in the supernatant.

Chapter 5
Discussion

5.1. Removal of nanoplastics: influence of coagulant type

The initial ζ-potential of the turbidity and SA-scenario was slightly higher and lower than the initial ζ-potential of the Schie water. However, all the initial values were in the range of -30 to -10 mV, indicating basic particle stability [56]. As in Schie water, theoretical $FeCl_3$, $AlCl_3$ and PAC doses were all able to reduce the ζ-potential to the optimum range for CF and particle destabilisation (0 to ± 5 mV) [56]. These ζ-potential values confirm that charge neutralisation is the most important coagulation mechanism for all coagulants, as suggested by literature (section 2.3.2). The $FeCl_3$ (and $AlCl_3$) experiments without pH adjustments suggest that sweep flocculation also plays a role in NP removal. The coagulant flocs that trap the impurities have a slower formation rate than flocs formed during charge neutralisation [44]. This explains why the flocs were visible after 24 hours, but not yet after 30 minutes. It is possible that this phenomenon was more outspoken for $FeCl_3$ than for $AlCl_3$ because the theoretical dose for Fe was so much higher than for Al [12, 13, 45] and/or because Fe-based coagulants are less soluble than Al-based coagulants [47]. This mechanism is less useful in practice since it requires long CFS times and high coagulant doses.

In the turbidity scenario, $FeCl_3$ (with pH adjustments) was the most efficient coagulant, followed by PAC and $AlCl_3$ (with pH adjustments) respectively. PAC obtained the highest R% in the SA scenario, followed by $FeCl_3$ and $AlCl_3$ respectively. These trends differ from observations made during the reference Schie water experiment (PAC > $AlCl_3$ > $FeCl_3$). However, operationally, the three coagulants are equally good, because the turbidity is reduced below 1 NTU in all cases. This was only the case for PAC in the Schie water experiment. In this scenario, with the theoretical optimum dose, the coagulants thus perform better for the removal of PS NPs than for the particulates in Schie water. This is most likely attributed to the fact that the particle composition in Schie water is more diverse and that NOM present in Schie water influences the floc formation [43].

In terms of NP R%, the difference in performance is more important. The NP R% in the turbidity equalled 95.30 %, 99.23 % and > 100 % for $AlCl_3$, PAC and $FeCl_3$. All NP R% were > 100 % for the SA scenario. NP R% above 100 % indicate that the final turbidity dropped below the initial tap water turbidity. Zhang et al. (2020) and Skaf et al. (2020) reported that Al-based coagulants are significantly better than Fe-based coagulants in the removal of MPs [21, 55]. Based on these results, this cannot be concluded for NP removal. $FeCl_3$ was most efficient in the turbidity scenario, but the three coagulants were equally efficient during the SA scenario.

Other process parameters, like alkalinity, pH and residual coagulants should also be considered when assessing the coagulant's performance. The initial alkalinity of the experiments was lower than the initial alkalinity for Schie water, but still sufficiently high to accommodate initial hydrolysis (> 50 mg $CaCO_3$/L [51]). Moreover, it was in the same range (75-112 mg $CaCO_3$/L) as the tap water used by Skaf et al. (2020) in their MP coagulation study [55]. The alkalinity drop was bigger than in Schie water for all the coagulants, but similar for the turbidity and SA scenario. As in Schie water, PAC consumed the least alkalinity, while $AlCl_3$ and $FeCl_3$ consumed a similar amount, confirming the different initial hydrolysis mechanisms. $AlCl_3$ and $FeCl_3$ form hydrolytes when they react with water, releasing hydrogen ions that react with the initial alkalinity and influence the pH. These reactions are less at play for the prehydrolysed PAC [13, 62].

PAC was the only coagulant that produced a supernatant with a final alkalinity (58 mg CaCO3/L) close to the proposed threshold (> 60 mg CaCO3/L) [64]. Moreover, PAC was the only coagulant that did not require pH adjustments to facilitate efficient CFS. The residual coagulant concentration exceeded the legal threshold for $AlCl_3$ in the turbidity scenario. This was also observed for the Schie experiment, however, the residual concentration in the NP experiment was higher than for the Schie experiment. The experiments with the other coagulants and the $AlCl_3$ SA scenario obey the threshold. The residual concentration for the PAC supernatant was (close to) exceeding the threshold for the Schie reference experiment but this was not the case for the NP experiments.

In conclusion, the experiments showed that charge neutralisation is the main coagulation mechanism for all three coagulants. Sweep flocculation is also involved for $FeCl_3$, but in practice, the influence of this mechanism will be probably minimal, since industrial CFS processes are not long enough for coagulant flocs to form and doses are generally lower. The NP R% are close to one another for all coagulants in the different scenarios. However, PAC is the only coagulant producing a supernatant obeying the guidelines for pH and alkalinity. No additional alkalinity needs to be added and no pH adjustments are required for distribution [51, 59]. Moreover, the residual coagulant concentrations are below the legal threshold in both scenarios. These findings therefore suggest that PAC is most efficient across different NP scenarios.

5.2.   Removal of nanoplastics: influence of coagulant dose

Like the theoretical optimum dose, the practical $AlCl_3$ and $FeCl_3$ doses were able to reduce the ζ-potential to the optimum range for CF and particle destabilisation (0 to ± 5 mV) [56]. This was not the case for the Schie water experiment and is most likely attributed to the more diverse particle composition in Schie water. As observed for the theoretical dose, $FeCl_3$ is more efficient than $AlCl_3$ for turbidity R% in both NP scenarios. Interestingly, the R% obtained in the turbidity scenario were almost equal to the R% obtained with the theoretical dose (> 90 %). This was different in the SA scenario (> 52 % versus > 87 %). Skaf et al. (2020) also observed higher R% for higher (25 mg/L, 99%) than lower (5 mg/L, 97%) MP concentrations [55].

The high particle concentration in the turbidity scenario likely introduced more collisions between the particles, leading to stronger and larger flocs that settled faster during sedimentation. The collision rate between coagulants and pollutants would have been lower for the SA scenario, resulting in smaller flocs [44]. Theoretically, micro-flocculation is the main flocculation mechanism for NPs, relying more on particle collision than on mixing [12]. This supports the hypothesis that variations in particle collision, and thus particle concentration, could have influenced the results. The difference between the R% in the two scenarios is smaller in the theoretical dose experiments. It is hypothesised that the theoretical dose is high enough to remove the lower NP concentration (SA scenario) through sweep flocculation. In both the turbidity and SA scenario, the NP R% was high with the practical dose, similar to the results with the theoretical dose. However, the SA scenario consistently showed lower NP R% than the theoretical dose, aligning with the general R% trend.

The residual coagulant concentration, alkalinity and pH do not indicate much difference between the two doses. The final alkalinity values are slightly higher for the practical dose, but still similar to the final alkalinity obtained with the theoretical dose. This was also observed in the Schie water experiments. Comparing pH values is difficult since the experiments with the theoretical dose required pH adjustments while the experiments with the practical dose did not. The residual coagulant concentration in both NP scenarios was equal to or lower than the residual concentration detected in the theoretical dose supernatant, so all the values obey the legal threshold. This was not the case for the reference Schie experiment.

Since the high NP concentrations in the turbidity scenario could have influenced the process, the SA experiment provides a more trustworthy way to compare the doses. Consequently, this research shows that theoretical (higher) doses are more efficient in NP R%. This is in line with what is suggested in MP and NP literature. Coagulation studies with $FeCl_3$ showed that doses higher than the general DWTP dose (110-280 mg Fe/L versus < 20 mg Fe/L) are more efficient for the removal of 0.5 mm PE MP (15 % versus 8 %) [8, 55]. Zhang et al. (2020) also report a higher MP R% (13.6 ± 6.8 %) for doses higher than the regular DWTP doses (< 5 %) [21].

Gong et al. (2022) used these three exact coagulants to coagulate 50 nm 50 mg/L PS-COOH and found maximum NP R% of 96.6 %, ~ 99% and 95.8 % for $AlCl_3$, PAC and $FeCl_3$ respectively. The doses required to achieve this optimum R% were higher for $AlCl_3$ and $FeCl_3$ (10 mg/L coagulant) than for PAC (5 mg/L coagulant) [6]. Ali et al. (2023) reported that $AlCl_3$ performed slightly better than $FeCl_3$ to coagulate 50 nm PS-COOH, confirming the findings by Gong et al. (2022) [2]. These NP R% are in the same order of magnitude as observed in this research. PAC was also identified as the most efficient coagulant because it had the highest NP R% at the lowest dose (in range of the practical dose). These results are not one-on-one comparable, since different and smaller plastic polymers were used [2, 20, 37] but support the conclusion that higher doses are more efficient for NP removal. A trade-off is that more sludge production will be produced if higher doses are used [13, 21]. Another trade-off is that CFS processes with $AlCl_3$ and $FeCl_3$ would require supernatant pH and alkalinity corrections, more for the higher theoretical dose than the lower practical one, which is in line with the findings by Pivokonsky et al. (2024) [13].

5.3. Removal of nanoplastics: influence of nanoplastic size

As mentioned, the influence of NP size was only investigated for PAC, considering dosage, obtained R% and temperature dependence. No noteworthy differences were observed between the different NP sizes concerning pH, alkalinity, or residual coagulant concentrations. Both the starting solutions and the supernatants showed similar pH and alkalinity for the different NP sizes and scenarios. The residual coagulant concentrations were below the detection threshold for all NP sizes and scenarios.

The NP_{200}, NP_{500} and NP_{1000} had different initial ζ-potentials, with the absolute ζ-potentials (SA scenario) decreasing with decreasing particle size. This observation is counter-intuitive, as smaller particles have a higher surface-to-volume ratio and a higher abundance of surface functional groups, they should have a higher charge density [7]. NP experiments in literature also describe a trend opposite to what was observed in this research. For example, Zhang et al. (2022) studied PS NP with a size between 50 and 1000 nm and observed that the absolute ζ-potential increased with decreasing NP size [3].

Additionally, the absolute ζ-potentials of NP_{200} and NP_{500} showed different values in the different NP concentration scenarios. Since the ζ-potential measures the charge of an individual particle [12], these values were expected to be the same for the same NP size regardless of the concentration. This discrepancy, in combination with the reversed trend, indicates that the initial ζ-potential measurements might not be accurate or that particles might already start to aggregate in the starting solutions. Aggregation could have changed the surface charge, thus explaining the reduced ζ-potential observed in smaller particles.

According to Zhang et al. (2022) NP_{1000} should be neutralised faster and more easily than smaller NPs due to the lower absolute ζ-potential. They observed that there is a stronger electrical repulsion between the smaller NPs and the coagulant (PAC), slowing down the coagulation process by weakening the neutralisation effect [3]. However, the final ζ-potentials measured in this research do not indicate such a trend. In the turbidity scenario, NP_{1000} was neutralised most effectively, followed by NP_{200} and NP_{500}. In the SA scenario, NP_{500} was neutralised best, followed by NP_{200} and NP_{1000}. However, the final ζ-potential values prove that the particles were effectively destabilised in all cases. Consequently, these results suggest that NP size does not seem to influence the charge neutralisation process.

The favourable ζ-potential values correspond to high turbidity R% (> 93 %) and NP R% (> 92 %) for all NP sizes in the two scenarios. The turbidity removal was highest for NP_{1000}, followed by NP_{500} and NP_{200} in the turbidity scenario. The same was observed in the SA scenario, but the R% for NP_{500} and NP_{200} were almost equal to one-another. NP_{1000} and NP_{200} had similar NP R% for the turbidity scenario (99%), while the NP R% for NP_{500} was slightly lower (96%). The observations for the SA scenario were similar, but the difference between NP_{1000}/NP_{200} (99%) and NP_{500} R% was bigger (92%).

Since charge neutralisation generally is the most common coagulation mechanism, the SA scenario was expected to allow a more uniform comparison between the NP sizes than the turbidity scenario, because the total available SA was different for each NP size in the turbidity scenario. However, even though the SA was kept the same, the particle concentration varied a lot and might have influenced the experiments. The NP_{200} particle concentration in the SA scenario was much higher (10^{11}) than for NP_{500} (10^{10}) and NP_{1000} (10^9). This means there would have been more particle collision for NP_{200} than for NP_{1000} and NP_{500}, possibly leading to more efficient CFS [44]. The comparison between sizes is thus less straightforward than for the previous experiments with the coagulants and only NP_{200}. An experiment with the same number of particles for each NP size is required to see if this difference in particle number have influenced the results.

Although there is no clear trend in these results, literature does suggest that particle size affects the MP/NP R% and settling behaviour [6]. Studies with PE MPs of 15-140 µm and 0.5-5 mm show that the MP R% decreases with increasing particle size [3, 55]. Experiments by Lapointe et al. (2020) confirm this: 500 MP/L were removed more efficiently with 2.73 mg AL/L and 0.3 mg PAM/L for 15 µm PE MPs (89%) than for 140 µm PE MPs (82%) [33]. This would be attributed to the fact that larger MPs are relatively larger than the average floc size, making it difficult to incorporate and easier to be rejected from the floc structure [3].

As this issue is not at play for smaller MPs, it should not influence NP removal. Zhang et al. (2022) performed experiments with 0.4 g PAC/L in combination with 20 mg PAM/L to remove PS NPs of different sizes. Contrary to the MP experiments, the NP R% significantly improved with increasing particle size (50 nm ~ 85.6 ± 0.2 %, 100 nm ~ 86.3 ± 0.2 %, 500 nm ~ 98.5 % ± 0.7 %, 1000 nm ~ 89.5 ± 1.1 %). Based on these results, Zhang et al. (2022) suggest that the ability to embed particles into flocs plays a significant role in the removal of large PE MPs, while the removal of smaller MPs and NPs is controlled by the particle's affinity with the coagulant and thus depends more on the charge neutralisation effect [3]. The NP_{500} particles are removed best in Zhang's study, while these particles are removed least efficiently during the two scenarios in this research. It is unclear what the NP concentrations were in the different solutions used by Zhang et al. (2022), which makes it difficult to make a direct comparison.

In conclusion, the inconsistencies between the findings from this study and previous studies do not allow to formulate a clear answer to the research question. Moreover, they highlight that there should be a better way of reporting NP concentration (particle- or mass-based) to accurately compare different studies. Experiments with equal numbers of particles for each NP size will be needed to determine if the big difference in particle concentration could have influenced the results and the outcomes discussed here.

5.4. Coagulation-flocculation-sedimentation of nanoplastics in Schie water

The original plan was to spike tap Schie water with a low concentration of NPs with palladium (Pd) inside. ICP-MS measurements would determine the NP concentration in the water by measuring the Pd concentration (0.1-10 µg/L). These experiments would have helped to validate the findings from the tap water experiments, by comparing the NP R% in a SW matrix (Schie) to the NP R% obtained in the tap water experiments. Due to insufficient Pd-NPs availability, these experiments were cancelled. Instead, the experiments were conducted with regular NP_{200}. Although it is not possible to distinguish between the particles naturally present in Schie water and the spiked NPs, and the turbidity is higher (13.85 NTU) than what the optimum dose was determined for (7.30 NTU), these experiments gave an indication of the influence of present NPs on CFS efficiency in a real SW matrix.

A huge alkalinity drop was observed after the Schie water was spiked with NPs (117 to 45 mg $CaCO_3$/L). According to literature, this starting alkalinity is insufficiently high to accommodate initial hydrolysis (> 50 mg$CaCO_3$/L [51]). However, the successful CFS suggest that this was not an issue in these experiments. Moreover, the starting pH was not affected by the addition of NPs and the final pH values were in range of what was previously observed in the other experiments, indicating a comparable buffer capacity (alkalinity). These alkalinity values had to be determined manually because the Titrino broke down at the end of the experimental period. Therefore, the suggestion is to repeat the experiment and verify these measurements before overanalysing these results.

The ζ-potential of the Schie water decreased with the addition of spiked NPs, but the standard deviation was big. This could suggest that the NPs interacted with particles in Schie water which caused a change in surface charge, destabilised the particles and possibly accelerated particle removal. This hypothesis aligns with findings by Zhang et al. (2022) [3]. However, since the equipment reports values based on a series of three measurements (100 runs) per sample [57, 58] another option could be that the standard deviation is a result from measuring the charge of a particle naturally present in Schie water one moment (-12.57 ± 0.81 mV), and measuring the charge of an NP_{200} (10.10 ± 0.79 mV) the other moment.

The supernatant ζ-potential had smaller standard deviations and were higher (absolute value) than observed during the Schie experiment without NPs. The theoretical dose achieves a better particle destabilisation than the practical dose for $AlCl_3$, but not for $FeCl_3$. This is interesting because the difference in dosed coagulant between theoretical and practical dose is higher for $FeCl_3$ than for $AlCl_3$. This observation could mean that Al-based coagulants are more efficient than Fe-based coagulants in destabilising and removing plastic particles, as was suggested for MPs [21, 55]. This, however, was not found in the tap water experiments during this research and is not reflected in the R% obtained. Another explanation could therefore be that the different coagulants have different dominant coagulation mechanisms in this scenario. Sweep flocculation is expected to play a role in CFS with $AlCl_3$ and especially $FeCl_3$, as was observed for the experiment assessing the influence of coagulant type. The sweep flocculation mechanism is more outspoken for higher theoretical doses, which could explain why $FeCl_3$ outperforms $AlCl_3$ in the experiments with the theoretical dose.

The theoretical $FeCl_3$ dose achieved a higher turbidity R% than $AlCl_3$, even though the ζ-potential measurements suggest that the particles would have been destabilised better with $AlCl_3$. $AlCl_3$ achieved higher turbidity R% when comparing the practical doses, but the ζ-potential values from $AlCl_3$ and $FeCl_3$ were about the same. Comparing the theoretical doses to the practical ones, the R% and the ζ-potentials confirm that the higher (theoretical) dose are more efficient in particle removal and destabilisation than the lower (practical) doses. PAC achieved the highest turbidity R% across all coagulants and doses, but it was not the coagulant with the lowest absolute ζ-potential. However, it is the only coagulant that reduced the residual turbidity below 1 NTU. The fact that PAC performs best is consistent with the findings in the Schie refence experiment and the tap water experiments.

Although the turbidity R% are lower than those observed in the tap water experiments, they are all equal (practical dose) or higher (theoretical dose) than the turbidity R% obtained in the reference Schie experiment. The lower R% in Schie water compared to tap water is most likely attributed to the presence of NOM [6]. The presence of humic acid (an important part of NOM), for example, is proven to inhibit the (PS NP) R% because of competitive adsorption. The available coagulant adsorption sites are preferably occupied by humic acids [3]. Studying MP removal in a DWT, Lapointe et al. (2020) observed that the profiles of turbidity R% were similar for SW and SW containing 500 PE MPs (140 µm) per litre [33]. This is a promising observation. The particles naturally present in Schie water made up 52.7 % of the experimental turbidity, while 47.3 % of the turbidity was introduced by the spiked NPs. The exact R% of the natural particles and the NPs cannot be determined, but the fact that the turbidity R% are higher than 52.7 % for all the coagulants for both doses strongly suggest that NP removal did occur. However, the final ζ-potential values also show that stable particles were left in the supernatant.

The trend observed for the residual coagulant concentration follows the observations from the reference Schie experiment. The residual Al concentration in the PAC experiment is again close to the threshold, which was the case for the Schie water experiment but not the case for the tap water experiments. Thus, although PAC seems to be most efficient across different conditions (highest R%, most favourable final alkalinity and pH values), there should be special attention to the residual coagulant concentration when DWTPs use PAC during CFS. Pivokonsky et al. (2024) observed that PAC doses that obtain an Al residual concentration below the threshold value were restricted to a narrower pH range compared to alum, $FeCl_3$ and $Fe_2(SO_4)_3$ [13].

In conclusion, this experiment confirmed that PAC is the most efficient coagulant across different water matrixes and NP concentrations, achieving the highest R% and favourable final alkalinity and pH values. As in the other experiments, higher theoretical doses outperformed lower practical doses, confirming the role of sweep flocculation alongside charge neutralisation. The current detection methods did not allow to determine NP R%, but the fact that observed turbidity R% were equal to or higher than the turbidity R% in unspiked Schie water is promising.

5.5. Coagulant composition and doses

A big challenge in CFS studies is how researchers report coagulant doses. The doses discussed in the Chapter 4 were given as concentration active ingredient (Al or Fe), but this is not always clear in other studies. When the dose is reported as coagulant per litre, it is difficult to correctly determine the concentration of the active ingredient because the actual characteristics of stock coagulants may differ from what is reported by manufacturers (Appendix E). However, even when studies would report coagulant doses as active coagulant concentration, the entire coagulant composition should not be forgotten.

Pivokonsky et al. (2023) performed different experiments with alum, PAC, $FeCl_3$ and $Fe_2(SO_4)_3$ on reservoir water used for DW production. Multiple differences in performance exist between these traditional coagulants. The anions (chloride or sulphate) included in the coagulant have a different influence on the CFS performance. Sulphate is considered to alter the coagulation more than chloride. The formed species are different, and the presence of sulphate can decrease the positive charge of the coagulant by adsorbing to the metal precipitate. This would result in faster aggregation and larger flocs over bigger pH ranges. These findings indicate that coagulants should not only be considered as Al- or Fe-based, but that the entire composition should be considered [13]. This makes it challenging to accurately compare findings from different studies.

5.6.　Experimental versus environmental (nano)plastics: properties and concentrations

The PS NPs used during this research are virgin or pristine particles. The properties of these virgin particles are different from the NP properties in natural environments. Plastic particles in the environment are typically weathered, vary in shape and material and have biofilms, NOM, or other contaminants attached to their surfaces [21, 29, 37, 65]. These interactions alter the characteristics of the particles [29, 37, 65], but different researchers suggest different effects of these alternations on the performance of DWTPs. Keerthana Devi et al. (2022) states that the alternations cause challenges for the performance of DWTPs [29] and Gong et al. (2022) observed that virgin PET-MPs had higher R% than aged PET-MPs [6]. On the contrary, Zhang et al. (2020) demonstrated in lab experiments that biofilms significantly enhanced the MP R% (0.3 ± 0.3 % to 16.5 ± 7.3 %). This was confirmed by repeating the experiment in a real DWTP (~ 5 % to 40.5–54.5 %) [21]. Similarly, another study found higher MP R% in DWTPs (64 %) than in lab-based CFS studies (0.1-1.2 %) [34].

There were no contaminants that could compete for coagulant during this research, because the NPs were spiked in tap water with a low initial turbidity. The water chemistry (pH, temperature, salinity and inorganic compounds) of tap water and SW differs and is known to affect the aggregation of NPs [6] and influence floc formation [43]. Some studies suggest that presence of NOM reduced NP R% [3], while other studies report that NOM enhances the NP R% by developing higher-quality flocs [6]. This could not be systematically investigated because of detection limitations of NPs in actual SW matrices, and because virgin particles do not account for these interactions, possibly over- or underestimating the NP R% in DW production.

Another issue in current research is that MP/NP concentrations are defined in multiple ways during different studies. NP concentrations are reported as mass (g/L) or number (particles/L) concentration [15]. For instance, Kumar et al. (2023) report MP particle concentrations in tap water of 0 to 60.9 items/L (100-5000 µm) [8] while Li et al. (2022) report an NP mass concentration of 1.67 to 2.08 µg/L for particles between 58-255 nm [10]. The concentrations of MPs and NPs in natural water bodies are estimated to be lower than 1 mg/L [2] and between 0.283 and 563 µg/L for NP specifically [15, 19].

The NP concentrations in this research are expressed as mass concentrations and are higher than those typically found in natural aquatic environments. This is not uncommon for experimental studies. Many studies have examined the transport and fate of NPs in aquatic environments at concentrations around 10 mg/L [15]. These high concentrations are required to ensure that the concentrations can be measured, because there are no established ways to measure particles this small [5, 21, 66]. Flow-cytometry is an emerging technique to measure NP concentrations for 150-200 nm particles, but the NPs need to be fluorescent or stained [10, 66]. Environmental samples need to be concentrated up to 10^8 times to meet the minimal NP detection limit of flow cytometry [30]. UV and turbidity are used in numerous studies. The LOD of UV was found to be higher than the LOD of turbidity, and many researchers highlight that turbidity is more sensitive than UV to measure NP concentrations [25, 33, 34, 55], which was also observed during this research. Moreover, these techniques do not allow to work in real SW matrices, because they cannot distinguish between different types of particles (turbidity) or because the baseline changes (UV blank).

The difference between the experimental NP concentration (< 2.36 mg/L) and the concentrations in natural water (< 563 µg/L) bodies could lead to different collision rates and different dominant CF mechanisms [44], resulting in R% different than what would be observed in natural settings. The fact that the particle concentration can make a difference is shown by the results of the tap water experiments with the practical $AlCl_3$ and $FeCl_3$ concentrations (turbidity and SA scenario). This difference in NP concentration has implications for the relevance and applicability of these findings to real-world scenarios and highlights a significant research gap. The residual NP concentration in some of the supernatants is higher than the concentrations reported in DW, and higher than the starting concentration for the DWTPs (SW concentration).

Chapter 6
Conclusions

This research aimed to provide a clear answer to how the coagulant type, coagulant dose and the particle size influence the removal efficiency of NPs during CFS processes. Three research questions guided this research:

RQ1: How do different coagulant types compare in removing nanoplastics?
RQ2: How does the variation in coagulant dose affect the nanoplastic removal efficiency?
RQ3: To what extent does variation in NP particle size affect the nanoplastic removal efficiency?

$AlCl_3$, PAC, and $FeCl_3$ were used as coagulants in this research. Theoretical doses were determined in Schie water based on ζ-potentials corresponding to -5 mV, while practical doses were determined based on a survey with four Dutch DWCs. The theoretical dose for PAC was in range with what the DWCs reported, which was not the case for $AlCl_3$ and $FeCl_3$. PAC achieved the highest turbidity R% for the reference Schie water experiment, and no alkalinity or pH corrections were required for the supernatant. However, the residual coagulant concentration was close to (exceeding) the legal threshold.

The influence of coagulant type and dose was tested with PS NP_{200} in two scenarios; turbidity based (7.5 NTU, 403 cm²/L and 1.41 mg/L) and SA based (135 cm²/L, 2.8 NTU, 0.47 mg/L). The theoretical dose of the coagulants achieved better turbidity R% in the experiments with NP-spiked tap water than in Schie water, for both the higher (turbidity scenario) and lower (SA scenario) NP concentrations. ζ-potential measurements confirmed that charge neutralisation is the most important coagulation mechanism for all the coagulants. Observed NP R% were high (> 95 %) for all coagulants, but considering the coagulation pH, the final pH, the final alkalinity, the required resources and the residual coagulant concentration, these experiments suggest that PAC is most efficient across different conditions. This was also confirmed in the experiment with spiked Schie water.

The experiment with the practical (lower) dose also gives additional insights into the theoretical dose experiment. Comparing the findings for the two doses showed that, next to charge neutralisation, sweep flocculation also contributes to the removal of NPs and that theoretical (higher) coagulant doses are therefore more efficient for NP removal. This was confirmed by the spiked Schie water experiment. More resources are required for the theoretical doses, since these doses require more coagulant and need pH adjustments to facilitate efficient CFS. However, these pH adjustments were not required to facilitate coagulation in the experiments with spiked Schie water, but adjustments would still be needed after CFS to increase the pH to > 7 before distribution.

PAC and PS NP_{1000}, NP_{500} and NP_{200} (turbidity and SA scenario) were used to investigate the impact of NP size variation on NP R%. No clear trend was observed in these experiments because the difference in particle number for each NP size introduced different collision rates, thereby influencing the micro-flocculation and eventually the results. Literature does suggest that particle size affects the MP and NP R%: larger MPs are primarily removed through their incorporation into flocs, while the removal of smaller MPs and NPs is more dependent on their affinity with the coagulant, relying heavily on charge neutralisation. However, the findings in this research were unable to confirm or refute these statements.

In conclusion, experiments with virgin PS NPs in tap water demonstrated that PAC was more efficient than $AlCl_3$ and $FeCl_3$ under various conditions. PAC achieved the highest R% and produced the most favourable final alkalinity and pH values, but crucial monitoring of the residual coagulant concentration is required. The study also found that theoretical coagulant doses resulted in better NP R% than the practical doses. Next to charge neutralisation, sweep flocculation also helps to increase the NP R%. It is important to note that higher coagulant doses will generate more sludge and require additional resources for dosing and pH adjustments. Lastly, no definitive conclusion was reached regarding the influence of NP size on R%.

It is important to remember that these findings are specific to the coagulants used in this research, i.e. AlCl₃, PAC, and FeCl₃. Care should be taken when comparing these findings to findings for other coagulants. The concentration of the active ingredient is important, but the entire coagulant composition should not be forgotten, since different anions can have a different influence on the performance. Next to that, it should not be forgotten that pristine NPs were used during this research and that the concentrations were higher than in the environment. The pristine NPs provide a controlled environment to study NPs, with uniform shape, size and material and without biofilms, NOM or other contaminants attached to the surface. However, it is crucial to acknowledge that these findings might therefore not fully represent the NP R% in more complex natural water matrices. This is an important gap between laboratory research and real-world DWT because there is currently no consensus in literature on how interactions enhance or decrease NP R%. The used NP concentrations were higher than in the environmental concentrations to allow particle detection with UV and turbidity. Experiments did show that different particle concentrations can result in different dominant coagulation and flocculation mechanisms and different R%. The difference in concentration thus has implications for the relevance and applicability of these findings to real-world scenarios.

Chapter 7
Limitations & Future recommendations

7.1. Nanoplastic properties beyond the lab

Ideally, real plastic polymers should be used instead of virgin NP particles with a perfect spherical size in future research. However, findings of experiments with weathered plastics might not be easy to generalise either. The surface of NPs strongly depends on the micro-environment, which causes the surface-dependent properties to vary in different settings [8]. Science still needs to find a consensus on how the interactions would influence the results obtained with virgin plastics [6, 21, 29].

Most lab studies use PS or PE particles because these are commercially available in virgin form, but PP and PET are also common. NP particles of 1000 nm, 500 nm and 200 nm were used in this research, but they were always used in homogenous solutions and never mixed. This does not represent the diversity of NPs found in the environment. Particles that are even smaller (58-255 nm) are most abundant in aquatic environments [10] and future research should therefore aim to include a broader range of NP types and sizes to enhance the validity of the findings. Moreover, other polymers should be tested too. Studies report a difference in R% for various polymers, even under identical conditions, due to differences in morphology, size, and type [2, 20, 37]. For example, Gao et al. (2022) reported that PS MPs could be removed (77.83 %) with PAC as a coagulant, while the coagulant was not efficient in removing PE MP particles [37]. Zhou et al. (2021) showed that PS MPs were removed for 77.83 % and 63 % by PAC and $FeCl_3$ respectively, while PE MPs were only removed for 29.70 % and 10 % [47].

7.2. (Overcoming) nanoplastic detection challenges

The biggest limitation of current NP research is the detection equipment. The fact that there is no established and easy way to measure the NP concentration is a bottleneck for all the research that is currently ongoing. Expensive fluorescent particles are required, or particles need to be strained following tedious staining procedures to detect them in low concentrations with flow cytometry [10, 66]. In case no flow cytometer is available, higher concentrations are required to detect the particles with different analytical techniques. It is not possible to use real SW matrices in that case. This has implications for the relevance of lab results to real-world scenarios.

The techniques used in this research, UV and turbidity, worked because the concentrations were high and the water matrix was tap water. The UV-VIS technique was less robust than turbidity because the colour introduced by the coagulants (especially $FeCl_3$) influenced the measurement and because the LOD was higher than for turbidity. UV-VIS can distinguish particles, but results showed that it cannot be used in more complex water matrices because of the required blank. The colour naturally present in Schie water was removed during the experiment, making the blank unrepresentative. Turbidity is not able to distinguish particles, but Lapointe et al. (2020) observed that the profiles of turbidity R% were similar for SW and SW containing 500 PE MPs (140 µm) per litre. This suggests turbidity could be used as indicator of plastic particle removal in DWTPs. However, for lab studies, the development of more advanced equipment is required before the NP experiments can be done in more relevant water matrices.

7.3.   (Standardising) nanoplastic concentration

There is no consensus on how to report the concentration of NPs, by mass concentration or by particle concentration. This makes the comparison of different results less straightforward and complicates the comparison of different NP sizes. This research chose to work with an NP mass concentration corresponding to a certain turbidity level and a certain SA value. This was interesting for the coagulant type and dose experiments with one NP size, but less so for the experiments with the different NP sizes. Different NP sizes have different turbidity calibration curves and different total available SAs. The different particle concentrations possibly influenced the results, because of different collision rates and different flocculation mechanisms. Future research must report the NP concentration as mass concentration and as particle concentration to increase the interpretability of the results.

7.4.   Alternative coagulants, flocculants and standardised dosage reporting

This study and other studies in literature mostly focussed on a limited number of coagulants. Although these coagulants are most common in DWTPs, it might be relevant to consider other commercially available coagulants that have been proposed as cost-effective for water treatment (e.g. plant-based coagulants) [6]. For the more common Al- and Fe-based coagulants it could be helpful to standardise the reporting of dosage as active ingredient, to facilitate easier comparison between different studies and DWTP practice. This research did not study how the addition of flocculant aids changes the process efficiency. Since the Dutch DWCs indicate that they use Wisprofloc N as flocculant aid during winter this would be relevant to investigate in the future. Some studies in literature already used PAM and PolyDADMAC.

7.5.   From (standardised) experimental conditions to full-scale operation

JT procedures normally mimic the conditions corresponding to the conditions at the WTP, but the procedure during this research was standardised for all coagulants, to keep the experimental conditions the same. However, literature reports that Al- and Fe-based coagulants have different optimal slow and rapid flocculation mixing rate [13]. Repeating the experiments with these optimal settings for the different coagulants, or the settings at a specific DWC, might influence the performance and change the findings. In general, even for regular coagulant and dose screening experiments, tests on full scale are required to validate findings in JTs [12]. Therefore, it is recommended that pilot studies are also done to verify these lab-based findings.

Moreover, the temperature during this research (19 °C) was higher than the average temperature in Dutch DWTPs (~ 12-15 °C). Temperature affects the solubility of coagulants and their hydrolysis rates. Al-based coagulants are more sensitive to temperature changes than Fe-based coagulants [13, 51] but prehydrolysed coagulants like PAC should be most temperature-independent [12, 43, 45]. Most coagulants should perform well in water between 10 and 25 °C [13, 51], but it would be good to verify the results from this research at a temperature that corresponds better to the average temperature in Dutch DWCs

7.6.   Integrating the full treatment train and distribution network

The results of this research suggest that higher (theoretical) coagulant doses are more efficient in removing NPs than lower (practical) doses. However, before increasing the coagulant dose, the NP R% of the subsequent treatment steps should be considered. Section 2.2.2 discusses other techniques that might help remove MP/NPs. Kumar et al. (2023) have shown that the MP R% increased by adding more processes to the treatment train (70 % CF + SF, 81 % CFS + SF, 83 % CF + flotation + SF + AC) [8]. It might therefore be unnecessary to increase the coagulant dose (and produce more sludge) if the entire treatment train together can remove all MPs/NPs. Integration studies with e.g. adsorption, photocatalysis, advanced oxidation process, DAF, and membrane filtration would be needed to evaluate this.

The obtained NP R% in this research were high and suggested almost complete removal of NPs during CFS. However, NPs are being detected in finished DW [8]. It would be beneficial to evaluate the techniques and material used in the entire DWTP treatment train, to make sure plastic pipes, filtration membranes, or other polymer-based materials used in DWTPs and distribution networks do not release NPs due to aging, friction or chemical reactions over time [10].

Reference List

1. DrinkwaterPlatform. *Waar komt ons drinkwater vandaan?* 2021 [cited 2024 27 March]; Available from: https://www.drinkwaterplatform.nl/themas/watertransitie/winningen/.

2. Ali, I., et al., *Recent innovations in microplastics and nanoplastics removal by coagulation technique: Implementations, knowledge gaps and prospects.* Water Research, 2023. **245**: p. 120617.

3. Zhang, Y., et al., *Improving nanoplastic removal by coagulation: Impact mechanism of particle size and water chemical conditions.* Journal of Hazardous Materials, 2022. **425**: p. 127962.

4. HeinrichBöllStiftung and BreakFreeFromPlastic, *The PLASTIC ATLAS 2019*. 2019.

5. Gambino, I., et al., *Occurrence of Microplastics in Tap and Bottled Water: Current Knowledge.* Int J Environ Res Public Health, 2022. **19**(9).

6. Gong, Y., et al., *Aggregation of carboxyl-modified polystyrene nanoplastics in water with aluminum chloride: Structural characterization and theoretical calculation.* Water Research, 2022. **208**: p. 117884.

7. Chen, Z., et al., *Nanoplastics are significantly different from microplastics in urban waters.* Water Research X, 2023. **19**: p. 100169.

8. Kumar, L.R., et al., *Chapter 8 - Microplastics and nanoplastics in drinking water and food chain*, in *Current Developments in Biotechnology and Bioengineering*, R.D. Tyagi, et al., Editors. 2023, Elsevier. p. 183-200.

9. National Academies of Sciences, E. and Medicine, *Environmental Engineering for the 21st Century: Addressing Grand Challenges*. 2019, Washington, DC: The National Academies Press. 124.

10. Li, Y., Z. Wang, and B. Guan, *Separation and identification of nanoplastics in tap water.* Environ Res, 2022. **204**(Pt B): p. 112134.

11. Pulido-Reyes, G., et al., *Nanoplastics removal during drinking water treatment: Laboratory- and pilot-scale experiments and modeling.* Journal of Hazardous Materials, 2022. **436**: p. 129011.

12. Crittenden, J.C., et al., *Coagulation and Flocculation*, in *MWH's Water Treatment: Principles and Design, Third Edition*. 2012. p. 541-639.

13. Pivokonsky, M., et al., *Fundamental chemical aspects of coagulation in drinking water treatment – Back to basics.* Journal of Water Process Engineering, 2024. **57**: p. 104660.

14. Letcher, T.M., *Chapter 1 - Introduction to plastic waste and recycling*, in *Plastic Waste and Recycling*, T.M. Letcher, Editor. 2020, Academic Press. p. 3-12.

15. Xu, Y., et al., *Identification and Quantification of Nanoplastics in Surface Water and Groundwater by Pyrolysis Gas Chromatography-Mass Spectrometry.* Environ Sci Technol, 2022. **56**(8): p. 4988-4997.

16. Napper, I.E. and R.C. Thompson, *Plastic Debris in the Marine Environment: History and Future Challenges.* Glob Chall, 2020. **4**(6): p. 1900081.

17. Geyer, R., *Chapter 2 - Production, use, and fate of synthetic polymers*, in *Plastic Waste and Recycling*, T.M. Letcher, Editor. 2020, Academic Press. p. 13-32.

18. Mariano, S., et al., *Micro and Nanoplastics Identification: Classic Methods and Innovative Detection Techniques.* Frontiers in Toxicology, 2021. **3**.

19. Materić, D., et al., *Presence of nanoplastics in rural and remote surface waters.* Environmental Research Letters, 2022. **17**(5): p. 054036.

20. Râpă, M., et al., *Insights into Anthropogenic Micro- and Nanoplastic Accumulation in Drinking Water Sources and Their Potential Effects on Human Health.* Polymers, 2023. **15**(11): p. 2425.

21. Zhang, Y., et al., *Removal efficiency of micro- and nanoplastics (180 nm–125 µm) during drinking water treatment.* Science of The Total Environment, 2020. **720**: p. 137383.

22. Sharma, V.K., et al., *Environmental factors-mediated behavior of microplastics and nanoplastics in water: A review.* Chemosphere, 2021. **271**: p. 129597.

23. Chen, Z., et al., *Phase transition of Mg/Al-flocs to Mg/Al-layered double hydroxides during flocculation and polystyrene nanoplastics removal.* Journal of Hazardous Materials, 2021. **406**: p. 124697.

24. MacLeod, M., et al., *The global threat from plastic pollution.* Science, 2021. **373**(6550): p. 61-65.

25. Abi Farraj, S., et al., *Targeting nanoplastic and microplastic removal in treated wastewater with a simple indicator.* Nature Water, 2024. **2**(1): p. 72-83.

26. Ter Halle, A., et al., *Nanoplastic in the North Atlantic Subtropical Gyre.* Environmental Science & Technology, 2017. **51**(23): p. 13689-13697.

27.   Cook, C.R. and R.U. Halden, *Chapter 20 - Ecological and health issues of plastic waste*, in *Plastic Waste and Recycling*, T.M. Letcher, Editor. 2020, Academic Press. p. 513-527.

28.   Moon, S., et al., *Direct observation and identification of nanoplastics in ocean water.* Science Advances, 2024. **10**(4): p. eadh1675.

29.   Keerthana Devi, M., et al., *Removal of nanoplastics in water treatment processes: A review.* Science of The Total Environment, 2022. **845**: p. 157168.

30.   Li, J., et al., *Separation and flow cytometry analysis of microplastics and nanoplastics.* Front Chem, 2023. **11**: p. 1201734.

31.   RIVM. *Wettelijke eisen aan drinkwater*. 2023   [cited 2024 March 12]; Available from: https://www.rivm.nl/drinkwater/drinkwater-en-regelgeving#:~:text=De%20wettelijke%20kwaliteitseisen%20voor%20drinkwater,gebaseerd%20op%20de%20Europese%20Drinkwaterrichtlijn%20.

32.   EuropeanUnion, *DIRECTIVE (EU) 2020/2184 OF THE EUROPEAN PARLIAMENT AND OF THE COUNCIL of 16 December 2020 on the quality of water intended for human consumption (recast)* 2020: Official Journal of the European Union.

33.   Lapointe, M., et al., *Understanding and Improving Microplastic Removal during Water Treatment: Impact of Coagulation and Flocculation.* Environmental Science & Technology, 2020. **54**(14): p. 8719-8727.

34.   Arenas, L.R., S.R.Z. Gentile, S., and S. Stoll, *Fate and removal efficiency of polystyrene nanoplastics in a pilot drinking water treatment plant.* Science of The Total Environment, 2022. **813**: p. 152623.

35.   Evides. *De zuiveringsprocessen*. 2021   [cited 2021 5 November]; Available from: https://www.evides.nl/drinkwater/de-zuiveringsprocessen.

36.   Madsen, H.T., *Chapter 6 - Membrane Filtration in Water Treatment – Removal of Micropollutants*, in *Chemistry of Advanced Environmental Purification Processes of Water*, E.G. Søgaard, Editor. 2014, Elsevier: Amsterdam. p. 199-248.

37.   Gao, W., et al., *Removal of microplastics in water: Technology progress and green strategies.* Green Analytical Chemistry, 2022. **3**: p. 100042.

38.   Lu, S., et al., *Removal characteristics and mechanism of microplastics and tetracycline composite pollutants by coagulation process.* Science of The Total Environment, 2021. **786**: p. 147508.

39.   Rezakazemi, M., A. Khajeh, and M. Mesbah, *Membrane filtration of wastewater from gas and oil production.* Environmental Chemistry Letters, 2018. **16**(2): p. 367-388.

40.   Guo, W.S., H.H. Ngo, and J.X. Li, *A mini-review on membrane fouling.* Bioresource Technology, 2012. **122**: p. 27-34.

41.   Dotto, G.L. and G. McKay, *Current scenario and challenges in adsorption for water treatment.* Journal of Environmental Chemical Engineering, 2020. **8**(4): p. 103988.

42.   Pillai, S.B., *Adsorption in Water and Used Water Purification*, in *Handbook of Water and Used Water Purification*, J. Lahnsteiner, Editor. 2020, Springer International Publishing: Cham. p. 1-22.

43.   Pivokonský, M., et al., *Jar Tests for Water Treatment Optimisation: How to Perform Jar Tests – a handbook*. 2022: IWA Publishing.

44.   Alazaiza, M., et al., *Application of Natural Coagulants for Pharmaceutical Removal from Water and Wastewater: A Review.* Water, 2022. **14**.

45.   AmericanWaterWorksAssosciation, *Operational Control of Coagulation and Filtration Processes*. 2011.

46.   Esfandiari, A. and D. Mowla, *Investigation of microplastic removal from greywater by coagulation and dissolved air flotation.* Process Safety and Environmental Protection, 2021. **151**: p. 341-354.

47.   Zhou, G., et al., *Removal of polystyrene and polyethylene microplastics using PAC and FeCl3 coagulation: Performance and mechanism.* Science of The Total Environment, 2021. **752**: p. 141837.

48.   Zhang, Y., et al., *Enhanced removal of polyethylene terephthalate microplastics through polyaluminum chloride coagulation with three typical coagulant aids.* Science of The Total Environment, 2021. **800**: p. 149589.

49.   Hogan, J., A. Morfesis, and U. Nobbmann, *Relating zeta-potential to jar testing, a comparison of two methods to optimize water treatment plant operation*. n.d., Malvern Panalytical.

50.   Kamble, S., et al., *Revisiting Zeta Potential, the Key Feature of Interfacial Phenomena, with Applications and Recent Advancements.* ChemistrySelect, 2022. **7**(1): p. e202103084.

51.   Greville, S.G., *How to select a chemical coagulant and flocculant*. 1997, Alberta Water & Wastewater Operators Association.

52.   VELPScientifica, *JLT4-JLT6 Flocculators Instruction Manual*.

53.   ThermoFisherScientific, *Turbidity units - a cloudy issue*. 2022.
54.   HACH. *What is the difference between the turbidity units NTU, FNU, FTU, and FAU? What is a JTU?* 2022; Available from: https://support.hach.com/myhach/s/article/KA-en-US-TE407-1000336?language=en_US.
55.   Skaf, D.W., et al., *Removal of micron-sized microplastic particles from simulated drinking water via alum coagulation.* Chemical Engineering Journal, 2020. **386**: p. 123807.
56.   Kumar, A. and C.K. Dixit, *3 - Methods for characterization of nanoparticles*, in *Advances in Nanomedicine for the Delivery of Therapeutic Nucleic Acids*, S. Nimesh, R. Chandra, and N. Gupta, Editors. 2017, Woodhead Publishing. p. 43-58.
57.   Malvern, *Zetasizer Nano User Manual* 2013, Malvern Instruments Ltd.
58.   Tang, J.A., *Malvern Zetasizer Nano User Manual* 2022, NYU Department of Chemistry
59.   Overheid.nl, *Drinkwaterbesluit*. 2024: Overheid.nl.
60.   Edzwald, J.K., *Aluminum in Drinking Water: Occurrence, Effects, and Control.* Journal AWWA, 2020. **112**(5): p. 34-41.
61.   TUDelftWaterlab, *Standard Operating Procedure ICP-OES*. 2023, TU Delft: Brightspace.
62.   VSSUT, *Environmental Engineering (Lab Manual)*. n.d., Veer Surendra Sai University of Technology Burla
63.   Crittenden, J.C., et al., *Physical and Chemical Quality of Water*, in *MWH's Water Treatment: Principles and Design, Third Edition*. 2012. p. 17-71.
64.   Dunea. *Bedrijfstechnische parameters*. [cited 2024 13 May]; Available from: https://www.dunea.nl/drinkwater/waterkwaliteit-en-samenstelling/verschillende-normen/bedrijfstechnische-parameters#Temperatuur.
65.   Rajala, K., et al., *Removal of microplastics from secondary wastewater treatment plant effluent by coagulation/flocculation with iron, aluminum and polyamine-based chemicals.* Water Research, 2020. **183**: p. 116045.
66.   Bianco, A., et al., *Rapid detection of nanoplastics and small microplastics by Nile-Red staining and flow cytometry.* Environmental Chemistry Letters, 2023. **21**(2): p. 647-653.
67.   Schaap, M. and R. Schots, *Waterbedrijf Groningen - Questionnaire coagulation and filtration process* 2023.
68.   Pieterse, B., *Dunea - Questionnaire coagulation and filtration process* 2024.
69.   de Ridder, D., *Evides - Questionnaire coagulation and filtration process* 2024.
70.   van Schooten, F., *Waternet - Questionnaire coagulation and filtration process* 2024.
71.   ThermoFisherScientific. *Aluminum chloride, anhydrous, granular, 99%*. Available from: https://www.thermofisher.com/order/catalog/product/A11892.0B?SID=srch-srp-A11892.30.
72.   VWR Chemicals. *Iron(III) chloride 41% in aqueous solution*. Available from: https://nl.vwr.com/store/product/2345714/iron-iii-chloride-41-in-aqueous-solution-technical.

Appendices

A. Survey with Dutch drinking water companies

Tabel A- 1: Survey with Waterbedrijf Groningen, Dunea, Evides and Waternet.

	Waterbedrijf Groningen[67]	Dunea[68]	Evides[69]	Waternet[70]
Water source and treatment steps				
Water source	Drentsche Aa	Pretreated dammed Meuse water	Meuse water pretreated in the Biesbosch reservoir	Lek river
Turbidity [NTU]	Min: <0.1 Avg: 11.1 Max: 30	Min: - Avg: 10.9 Max: -	Min: 0.7 Avg: 2.0 Max: 5.5	Min: - Avg: 8.1 Max: -
pH [-]	Min: 7 Avg: 7.6 Max: 8.2	Min: 8 Avg: - Max: 8.5	Min: 7.9 Avg: 8.7 Max: 9.3	Min: - Avg: 8.1 Max: -
ζ-potential [mV]	-	-	-	-
Temperature [°C]	Min: 0 Avg: 12.2 Max: 25	Min: 4 Avg: 13.5 Max: 25	Min: 2.6 Avg: 12.6 Max: 23.5	Min: - Avg: 14.8 Max: -
Treatment steps	60 days in retention basin Coagulation, flocculation Lamella sedimentation Dual-layer rapid sand filtration AC filtration UV disinfection Slow sand filtration Aeration & pH adjustment Potable water tank	Coagulation w/ $FeSO_4$ in the river Sedimentation in the dammed Meuse Microsieves (April-Oct) Inline coagulation Rapid sand filtration Dunes Softening Powdered activated carbon dosing Inline coagulation Rapid sand filtration and slow sand filtration	Coarse strainer Coagulation, flocculation Lamella separation Dual-layer rapid sand filtration Medium pressure UV Activated carbon filtration	Water intake Coagulation, flocculation, sedimentation Rapid sand filtration

Coagulation				
Type	-	Inline coagulation, direct rapid sand filtration	Coagulation, flocculation, sedimentation	Coagulation, flocculation, sedimentation
Goal	NTU & DOC removal, UV254nm < 14.5	Remove suspended solids < 0.5 mg/L	DOC, NTU, suspended solids, algae and UV transmission removal	Remove NOM and NTU
Turbidity [NTU]	Min: 1 Avg: 6 Max: 20.1	Min: - Avg: - Max: -	Min: 0.7 Avg: 2.0 Max: 5.5	Min: - Avg: 8.1 Max: -
pH [-]	Min: 7.6 Avg: 7.9 Max: 8.6	Min: - Avg: - Max: -	Min: 7.9 Avg: 8.7 Max: 9.3	Min: - Avg: 8.1 Max: -
ζ-potential [mV]	-	-	-	-
Temperature [°C]	Min: 2.4 Avg: 12.7 Max: 24.1	Min: - Avg: - Max: -	Min: 2.6 Avg: 12.6 Max: 23.5	Min: - Avg: 14.8 Max: -
Timing	43 min	-	40 min	-
Mixing	Waterfall mixing during coagulant mixing, 4 chambers with subsequent lower rotation speed and 4 horizontal mixers each	-	Rotation velocity of the flocculators is adjusted based on the water temperature	-
Coagulant	Poly Aluminium Chloride (PAC) Sachtoklar	Iron chloride	Iron chloride	Iron chloride
Dose summer	5-7 mgAl/L	-	5 mgFe/L	2.7 mgFe/L
Dose winter	7-9 mgAl/L	0.2-1 mgFe/L	5 mgFe/L + Wispro	2.7 mgFe/L
pH adjustment	7.1-7.3 before PAC dosing w/ HCl 6.8-7.0 after PAC dosing w/ HCl 6.5-7.0 after sedimentation w/ HCl	None	Not before coagulation, flocculation and sedimentation. Dosing NaOH before distribution.	None
Flocculation				
Flocculant aid	Wisprofloc N	None	Wisprofloc N	None
Dose summer	-	-		-
Dose winter	1-2 mg/L dissolved powder	-	0.5 mg/L	-
After the coagulation, flocculation, sedimentation process				
Turbidity [NTU]	0.2-0.6	0.7-1	0.4	-
ζ-potential [mV]	-	-	-	-
Adjustments when target quality is not met	Adjusting PAC dosing	Adjusting iron dose or filtration velocity	Adjusting iron or Wispro dose	-

B. Chemicals, materials and equipment

Tabel A- 2: Overview of the chemicals used in this research.

Chemical	Chemical formula	Supplier	CAS/Product number
Aluminium chloride, anhydrous, granular, 99%	$AlCl_3$	Alfa Aesar GmbH & Co KG	CAS: 7446-70-0
Hydrochloric acid	HCl	Carl Roth GmbH	CAS: 7647-01-0
Iron(III)chloride about 40%	$FeCl_3$	VWR® BDH® Chemicals	CAS: 7705-08-0
Micro particles based on polystyrene 1 µm	-	Sigma-Aldrich®	Product: 89904
Micro particles based on polystyrene 200 nm	-	Sigma-Aldrich®	Product: 69057
Micro particles based on polystyrene 500 nm	-	Sigma-Aldrich®	Product: 59769
Nitric acid ROTIPURAN®Ultra 69%	HNO_3	Carl Roth GmbH	CAS: 7697-37-2
Polyaluminium chloride, Sachtoklar®	-	Sample from Drinkwaterbedrijf Groningen	CAS: 39290-78-3
Sodium hydroxide	NaOH	Sigma-Aldrich®	CAS: 1310-73-2

Tabel A- 3: Overview of the materials used in this research.

Material	Supplier
StabCal® calibration Set 0 to 4000 NTU	HACH®
30 mL BD Luer-Lok™ Syringe	BD Plastipak™
CHROMAFIL®Xtra PES-20/25 disposable syringe filter, polyethersulfone	Macherey-Nagel GmbH & Co. KG
CHROMAFIL®Xtra PES-45/25 disposable syringe filter, polyethersulfone	Macherey-Nagel GmbH & Co. KG

Tabel A- 4: Overview of the equipment used in this research.

Equipment	Supplier
2100N Turbidimeter	HACH®
5800 ICP-OES	Agilent
702 SM Titrino	Metrohm
G1500+GE 114 pH-meter	Greisinger
GENESYS 10S UV-VIS Spectrophotometer	Thermo Fisher Scientific
JLT6 Flocculation Tester	VELP® Scientifica
Litesizer DLS 700	Anton Paar GmbH
Zetasizer Nano ZS	Malvern

C. Sphere calculations

Different values need to be calculated to determine the particle number per litre and the corresponding surface area (summary Tabel A- 5). The first step is to determine the mass (Equation A- 1), volume (Equation A- 2) and the surface area (Equation A- 3) of a single sphere. These values can be calculated with the particle size (200, 500 and 1000 nm) and the material density (1.05 g/cm²) as reported by the manufacturer. The experimental concentration and the mass allow to calculate the number of particles per litre (Equation A- 4), which can be converted to a SA per litre (Equation A- 5).

The particle mass concentration corresponding to 7.5 NTU was determined from the NP calibration curves (Appendix D). This concentration was translated to a certain particle number per litre and a certain SA per litre. The steps were reversed for the second scenario where the SA had to be 135 cm²/L in all experiments. From this, the experimental mass concentration could be determined. The mass concentrations were used to calculate how much (volume) NP solution had to be spiked in the tap water.

Equation A- 1: Mass of one sphere

$m_{sphere\,(mg)} = V_{sphere} * \rho_{material}$ with $\rho_{material}$ = material density [g/cm²]

Equation A- 2: Volume of one sphere

$V_{sphere}\,(cm^3) = \frac{4}{3} * \pi * r^3$ with r = sphere radius [cm]

Equation A- 3: Surface area of one sphere

$A_{sphere}\,(cm^2) = 4 * \pi * r^2$ with r = sphere radius [cm]

Equation A- 4: Number of particles per litre

$Particles\,per\,liter\,(\frac{\#particles}{L}) = \frac{C_{particle}}{m_{sphere}}$ with $C_{particle}$ = particle mass concentration [mg/L]

Equation A- 5: Surface area per litre

$Surface\,area\,per\,liter\,(\frac{cm^2}{L}) = particles\,per\,liter * A_{sphere}$

Tabel A- 5: Size, surface area, volume and mass per sphere for the different particles.

	Unit	NP$_{1000}$	NP$_{500}$	NP$_{200}$
Density material	g/cm³	1.05	1.05	1.05
Size/sphere	nm	1000	500	200
	cm	0.0001	0.00005	0.00002
Surface area/sphere	nm²	3141592.654	785398.2	125663.7
	cm²	3.14159×10^{-08}	7.85×10^{-09}	1.26×10^{-09}
Volume/sphere	nm³	523598776	65449847	4188790
	cm³	5.23599×10^{-13}	6.54×10^{-14}	4.19×10^{-15}
Mass/sphere	g	5.49779×10^{-13}	6.87×10^{-14}	4.4×10^{-15}
	mg	5.49779×10^{-10}	6.87×10^{-11}	4.4×10^{-12}
Surface/Volume ratio	1/nm	0.006	0.012	0.03
	1/cm	60 000	120 000	300 000
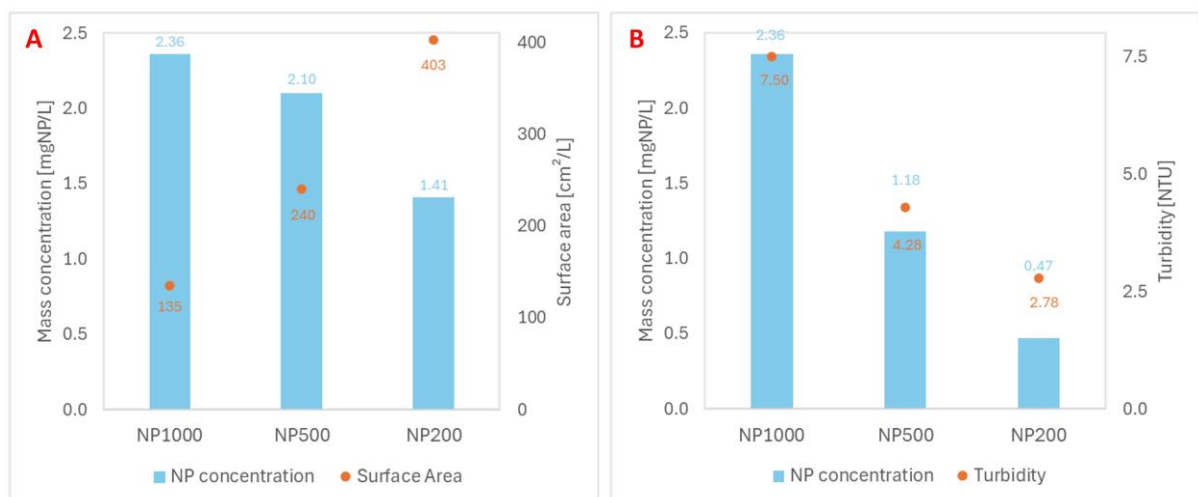
Figure A- 1: Sphere calculations and scenarios.

D. Particle calibration curves

Calibration curves for UV-VIS and turbidity were made for the different particles. The calibration curves are valid for concentrations between 0-3 mg NP/L. UV-VIS measurements were done at the peak wavelength of 298 nm. The sample analysis results in a simple linear data set. The linear trendline (y = ax + b) and the trendline reliability (R^2) were generated with Excel. y represents the sample turbidity (NTU) or the absorbance (cm^{-1}). x represents the particle concentration, in mg/L. The turbidity of the tap water equalled 0.3 NTU. The absorbance was set to zero by using tap water as the blank. A summary of the linear trendline equations is given in Tabel A- 6.

Tabel A- 6: Linear equation parameters (y = ax + b) of the calibration curves of the different nanoplastics.

Particle	a	b	R^2
Turbidity			
NP_{200}	5.0316	0.3997	0.9979
NP_{500}	3.5025	0.1456	0.9994
NP_{1000}	3.1102	0.1572	0.9998
UV-VIS			
NP_{200}	0.0266	0.0009	0.9917
NP_{500}	0.0286	0.0017	0.9942
NP_{1000}	0.0078	-0.0011	0.9833

E. Coagulant characterisation

The type of provided product information is different for different coagulants and differs per manufacturer. It is therefore not always straightforward to determine the coagulant concentration and/or the concentration of the active ingredient with Equation 1 and Equation 2. The ICP-OES results confirmed the Fe- or Al-concentration in the working solutions, and all the coagulant doses mentioned in this research are therefore either mg Fe/l or mg Al/L. An overview of the manufacturer information is given in Tabel A- 7.

A coagulant concentration of 2416 g/L was obtained for $AlCl_3$ based on the provided MW, composition and density. The manufacturer claims that 20 % of the solution is the active ingredient Al, therefore the solution should contain 97.91 g Al/L. The ICP-OES results show that the working solution (2 % wt) contains 1.85 mg Al/L, which corresponds to 92.27 g Al/L (18.18 % Al) in the stock solution. Similarly, the calculations for $FeCl_3$ result in a coagulant concentration of 1647 g/L and an iron concentration of 226.77 g Fe/L (40 %). The ICP-OES results return an iron concentration of 2.18 g Fe/L for the working solution, meaning that the stock solution contains 33.37 % Fe (189.16 g Fe/L).

The total coagulant and Al-concentration cannot be determined for PAC Sachtoklar®, because the MW of this polymer is unknown and the composition is more complicated than for the other coagulants (%Al_2O_3 = 10.2 %, %Al = 5.4 %, %Cl = 9.0 %, %SO_4 = 3.0 %). The ICP-OES measurement returns a concentration of 38.38 mg Al/L (Al% = 17.85 %). PAC is used in undiluted form [12], so this is the concentration for both the stock and the working solution.

Tabel A- 7: Coagulant information provided by the manufacturer.

	Granular, anhydrous $AlCl_3$ [71]	$FeCl_3$ about 40% [72]	Sachtoklar® PAC [67]
Molecular weight (g/mol)	133.34	162.21	-
Density (g/mL)	2.44	1.42	1.20-1.30
Density measured (g/mL)	-	1.42	1.20
Composition	%Al = 20 % Purity = 99 %	%Fe = about 40 %	%Al_2O_3 = 10.2 %, %Al = 5.4 %, %Cl = 9.0 %, %SO_4 = 3.0 %

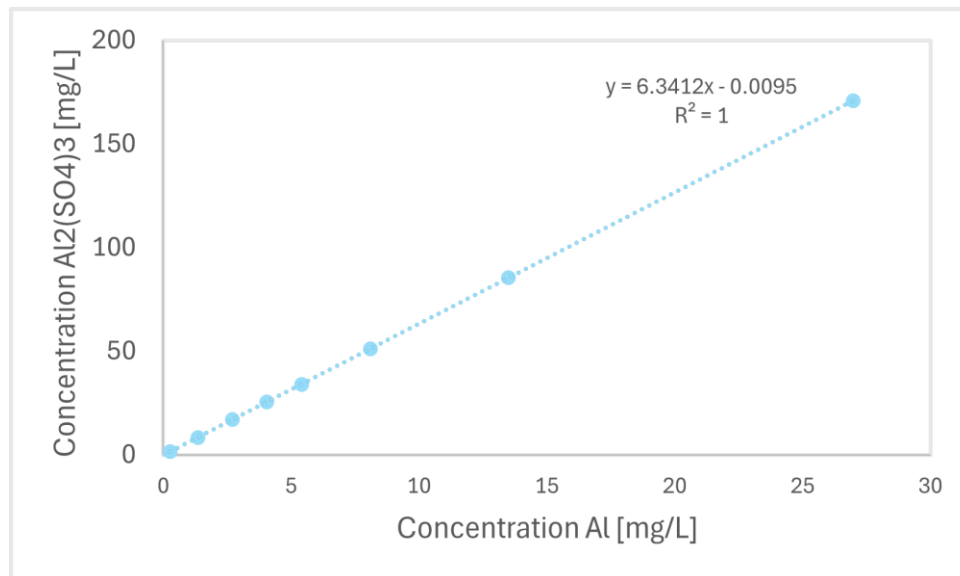## F. Conversion of mg Al$_2$(SO$_4$)$_3$/L to mg Al/L

Figure A- 2: Calibration curve used to determine practical AlCl3 dose.

G. Removal efficiencies and water quality parameters from the jar test experiments

Tabel A- 8: Removal efficiencies and water quality parameters for the reference Schie water experiment.

	Schie water experiment				
Parameter	FeCl$_3$ (Theoretical)	FeCl$_3$ (Practical)	AlCl$_3$ (Theoretical)	AlCl$_3$ (Practical)	PAC (Theoretical & practical)
Coagulant Dose [mg Fe/L or mg Al/L]	65.2	5	14.3	3.15	8.8
Initial Turbidity [NTU]	7.35 ± 0.071				
Residual Turbidity [NTU]	1.15 ± 0.07	1.56 ± 0.01	1.10 ± 0.08	1.46 ± 0.03	0.90 ± 0.08
Turbidity Removal Efficiency [%]	84.35 ± 0.96	78.70 ± 0.10	85.03 ± 1.11	80.14 ± 0.19	87.76 ± 1.11
Initial ζ-Potential [mV]	-12.57 ± 0.81				
Supernatant ζ-Potential [mV]	-4.48 ± 1.8	-11.2 ± 0.44	-0.98 ± 0.73	-9.87 ± 0.45	-4.95 ± 1.4
Initial Alkalinity [mg CaCO3/L]	177 ± 10.43				
Supernatant Alkalinity [mg CaCO3/L]	39 ± 0.18	41	49 ± 0.88	38	161 ± 9.53
Initial pH [-]	7.84				
Supernatant pH [-]	6.41 ± 0.06	7.72	6.37 ± 0.02	7.55	7.18 ± 0
Residual Coagulant [mg Fe/L or mg Al/L]	< 0.025	0.03 ± 0.00	0.03 ± 0.00	0.25 ± 0.01	0.27 ± 0.13

Tabel A- 9: Removal efficiencies and water quality parameters for the turbidity-based NP$_{200}$ experiment in tap water.

Parameter	FeCl$_3$ (Theoretical)	FeCl$_3$ (Practical)	AlCl$_3$ (Theoretical)	AlCl$_3$ (Practical)	PAC (Theoretical & Practical)
Experiment with NP200 in tap water (turbidity scenario)					
Coagulant Dose [mg Fe/L or mg Al/L]	65.2	5	14.3	3.15	8.8
Initial Turbidity [NTU]	6.89 ± 0.28				
Residual Turbidity [NTU]	0.55 ± 0.03	0.50 ± 0.04	0.71 ± 0.01	0.69 ± 0.07	0.46 ± 0.02
Turbidity Removal Efficiency [%]	92.76 ± 0.37	93.49 ± 0.47	89.77 ± 0.10	89.95 ± 0.97	94.01 ± 0.30
NP Removal Efficiency [%]	102.15 ± 0.10	98.68 ± 0.49	95.30 ± 0.11	94.86 ± 1.86	99.23 ± 0.30
Initial ζ-Potential [mV]	-14.23 ± 0.32				
Supernatant ζ-Potential [mV]	16.00 ± 2.01	-4.43 ± 0.35	5.40 ± 2.52	-0.53 ± 0.70	-1.57 ± 1.61
Initial Alkalinity [mg CaCO3/L]	103 ± 0.35				
Supernatant Alkalinity [mg CaCO3/L]	6	10	4	6	58
Initial pH [-]	7.51				
Supernatant pH [-]	6.98	6.95	6.78	6.95	6.78
Residual Coagulant [mg Fe/L or mg Al/L]	0.10 ± 0.00	0.02 ± 0.00	0.66 ± 0.01	0.05 ± 0.01	0.05 ± 0.00

Tabel A- 10: Removal efficiencies and water quality parameters for the surface area-based NP$_{200}$ experiment in tap water.

Parameter	FeCl$_3$ (Theoretical)	FeCl$_3$ (Practical)	AlCl$_3$ (Theoretical)	AlCl$_3$ (Practical)	PAC (Theoretical & Practical)
Experiment with NP200 in tap water (surface are scenario)					
Coagulant Dose [mg Fe/L or mg Al/L]	65.2	5	14.3	3.15	8.8
Initial Turbidity [NTU]	3.01 ± 0.02				
Residual Turbidity [NTU]	0.91 ± 0.06	1.29 ± 0.02	0.38 ± 0.02	1.45 ± 0.20	0.19 ± 0.01
Turbidity Removal Efficiency [%]	68.79 ± 2.19	55.69 ± 0.73	87.54 ± 0.71	51.74 ± 6.5	93.45 ± 0.49
NP Removal Efficiency [%]	106.19 ± 0.85	64.59 ± 0.85	100.95 ± 0.81	56.99 ± 7.04	108.39 ± 0.57
Initial ζ-Potential [mV]	-10.10 ± 0.79				
Supernatant ζ-Potential [mV]	19.97 ± 0.96	-1.13 ± 0.86	0.07 ± 0.06	-0.47 ± 0.21	-0.37 ± 0.38
Initial Alkalinity [mg CaCO3/L]	100 ± 0.53				
Supernatant Alkalinity [mg CaCO3/L]	5	13	4	8	57
Initial pH [-]	7.55				
Supernatant pH [-]	7.10	7.05	7.17	7.12	7.55
Residual Coagulant [mg Fe/L or mg Al/L]	0.00 ± 0.00	0.01 ± 0.00	0.07 ± 0.01	0.08 ± 0.01	0.07 ± 0.02

Tabel A- 11: Removal efficiencies and water quality parameters for the experiments with different NP sizes in tap water.

Parameter	NP200 (Turbidity)	NP200 (SA)	NP500 (Turbidity)	NP500 (SA)	NP1000 (Turbidity & SA)
Experiment with NP200, NP500 and NP1000 in tap water					
PAC Dose [mg Al/L]	8.8				
Initial Turbidity [NTU]	7.60 ± 0.04	2.9 ± 0.00	7.65 ± 0.08	4.49 ± 0.06	7.38 ± 0.01
Residual Turbidity [NTU]	0.46 ± 0.02	0.19 ± 0.01	0.35 ± 0.07	0.29 ± 0.04	0.21 ± 0.02
Turbidity Removal Efficiency [%]	94.01 ± 0.49	93.45 ± 0.49	95.43 ± 0.06	93.65 ± 0.04	97.22 ± 0.29
NP Removal Efficiency [%]	99.23 ± 0.30	>100%	95.92 ± 1.41	91.99 ± 2.03	99.34 ± 0.29
Initial ζ-Potential [mV]	-14.23 ± 0.32	-10.10 ± 0.79	-19.00 ± 0.33	-14.93 ± 1.22	-18.10 ± 0.67
Supernatant ζ-Potential [mV]	-1.57 ± 1.61	-0.37 ± 0.38	-1.80 ± 1.97	-0.07 ± 0.06	-0.58 ± 1.04
Initial Alkalinity [mg CaCO3/L]	~100				
Supernatant Alkalinity [mg CaCO3/L]	58	58	58	57	55
Initial pH [-]	~7.6				
Supernatant pH [-]	~ 6.2 – 6.4				
Residual Coagulant [mg Al/L]	0.05 ± 0.00	0.07 ± 0.02	0.08 ± 0.00	0.07 ± 0.02	0.08 ± 0.02

Tabel A- 12: Removal efficiencies and water quality parameters for the experiment with NP200 spiked Schie water.

Parameter	FeCl3 (Theoretical)	FeCl3 (Practical)	AlCl3 (Theoretical)	AlCl3 (Practical)	PAC (Theoretical & Practical)
Experiment with NP200 in Schie water					
Coagulant Dose [mg Fe/L or mg Al/L]	65.2	5	14.3	3.15	8.8
Initial Turbidity [NTU]	13.85 ± 0.07				
Residual Turbidity [NTU]	1.11 ± 0.13	2.95 ± 0.05	1.83 ± 0.07	2.50 ± 0.08	0.74 ± 0.01
Turbidity Removal Efficiency [%]	91.99 ± 0.92	78.74 ± 0.36	86.79 ± 0.51	81.99 ± 0.56	94.66 ± 0.10
Initial ζ-Potential [mV]	-9.47 ± 3.14				
Supernatant ζ-Potential [mV]	-11.37 ± 0.85	-11.90 ± 1.92	-4.33 ± 0.31	-11.37 ± 0.25	-9.73 ± 1.47
Initial Alkalinity [mg CaCO3/L]	45				
Supernatant Alkalinity [mg CaCO3/L]	13	43	10	36	35
Initial pH [-]	7.84				
Supernatant pH [-]	6.42	7.79	6.75	7.72	7.07
Residual Coagulant [mg Fe/L or mg Al/L]	< 0.025	0.03 ± 0.00	0.10 ± 0.01	0.35 ± 0.00	0.21 ± 0.00